Res. Rep. Fac. Eng. Mie Univ., Vol. 29, pp. 65-72 (2004)

Original Paper

Novel negative electrode materials with high capacity density for further rechargeable lithium ion batteries

Y. Liu[a], T. Matsumura[a], A. Hirano[b], T. Ichikawa[b], N. Imanishi[b] and Y. Takeda[b]
([a] Satellite Venture Business Laboratory, [b] Department of Chemistry for Materials)

(Received October 20, 2004)

Abstract

Solid-state rechargeable batteries, especially, lithium ion batteries, are principle and promising power sources for a wide variety of electronics. Electrode material is a key for developing further lithium ion batteries, which are likely to require good reliability and high energy density. However, graphitic carbon that is currently used as negative electrode material in the commercial Li-ion batteries appears to be unsatisfied due to low theoretic capacity of 372 mAh g^{-1} and poor thermal stability under lithiated state. Therefore, there is even-increasing research in the feasibility of the replacement of graphitic anodes. By this motivation, a series of novel negative electrode materials that demonstrate extremely high capacities and different Li reactive mechanisms have been proposed in this group. In this paper, we present a brief introduction with respect to some recent results. In particular, the characterizations of these anode materials are described and discussed based on different electrolytes such as liquid and solid systems.

Key words: Power sources; Rechargeable lithium ion batteries; Negative electrode materials; Energy density; Working voltage; Capacity; Li reactive mechanisms.

Background

Search for new energy sources becomes an urgent challenge in our society and is greatly related to the technology development. Such energy requires high efficiency, convenient, pollution-free and safety. As alternative energy sources and energy storage media, batteries have many advantages and are principle and promising power sources for a wide variety of electronics, e.g., portable, entertainment, computing and telecommunication equipments, as well as electric vehicles (EV) and hybrid electric vehicles (HEV) [1]. A typical battery is composed of many electrochemical cells in series in terms of exporting-energy requirement. Single cell contains a positive electrode (cathode) and a negative electrode (anode), which are separated by an ionic-conducting but electron-insulating electrolyte. The working voltage of the cell is due to the potential difference between the cathode and the anode (both sources of chemical reactions). Furthermore, the chemical reactions processed in both cathode and anode can generate electrons and currents in case of an external circuit connection between the two electrodes. The amount of electrical energy produced by the battery is dependent on several key parameters such as working voltage (V) and specific capacity (Ah Kg^{-1}), both of which are linked directly to the chemistry of the system, and is expressed according to either per unit of weight (Wh kg^{-1}) or per unit of volume (Wh L^{-1}). At present, fuel cell, nickel metal hydride and lithium ion batteries are the major research and attract even-increasing attention. In particular, lithium ion batteries have a remarkable expansion and now supply over 63 % of the total portable battery market in worldwide (90% in Japan, data cited from 2001) [2]. This is attributed to that lithium ion cell has rather high working voltage and thus large energy density. There is a long historical development over 30 years for Li-battery technology. The initial motivation for using Li as anode in batteries is due to the fact that metallic lithium possess the most electropositive character (-3.04 V vs. standard hydrogen

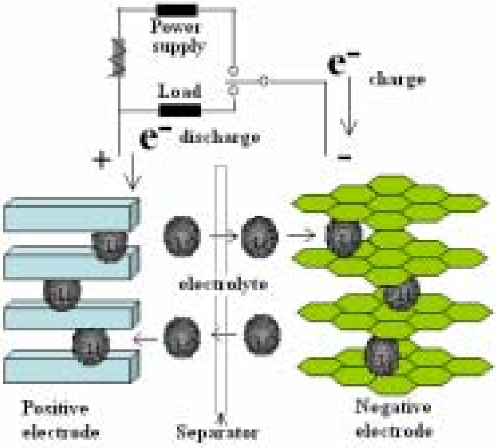

Fig.1. Principle of the lithium ion cell.

electrode) and the lightest weight (equivalent weight *M*= 6.94 g mol^{-1}, specific gravity ρ=0.53 g cm^{-3}), as well as the largest capacity density (ca. 3.8 Ah Kg^{-1}); thereby battery based on lithium anode shows very high discharge voltage and correspondingly large energy density. However, lithium dendrites that occur on the surface of the lithium anode during the repeated charge and discharge tend to cause a short current circuit and thereby a potential safety problem. Fortunately, this deterrent was tackled successfully by Sony Corporation, Japan, in June 1991, by introducing a kind of Li-intercalation host, such as graphite, in place of metallic lithium. Correspondingly, lithiated $LiCoO_2$ (lithium cobaltate) is adopted as cathode that gives high potential and acts as Li-sources. The "rocking chair" concept of the lithium ion cell proposed and commercialized firstly by Sony Corporation, as shown in Fig.1, make mobile Li^+ become shuttle between the cathode ($LiCoO_2$) and the anode (graphite) via the electrolytes in a charge and discharge process accompanied with an electrochemical electrode reaction. During the charging process under an applied external voltage, a certain amount of Li^+ are extracted from the cathode into the electrolyte, which is composed of lithium salt dissolved in a liquid solvent or a solid polymer/glass and is not consumed by the electrochemical charge–discharge reaction. Simultaneously, an equivalent amount of lithium ion are forced from the electrolytes intercalate into the graphite anode. The movement of the lithium ion during discharge is reverse to that of charge stage and is spontaneous. Charge compensation takes place through the external circuit during charge and discharge. By this way, the electrical energy can be saved during charging and released during discharging reversibly. The "rocking chair" manner highly avoids Li-dendrites and thus demonstrates high reliability. The currently commercial lithium ion cell consisting of $LiCoO_2$ and graphite has high discharge voltage of ca. 3.7 V and large energy density of ca. 110 Wh Kg^{-1}, which are apparently superior to those of Ni-Cd and Ni-MeH cells. Obviously, electrode materials that can reversibly storage lithium ion are the key for developing further lithium ion batteries. The research in the cathode that must possess high electrode potential mostly focuses on how to improve the electrode capacity, which is below to 200 mAh g^{-1} in the current system, indicating that the weight of cathode to anode must be over 2 times. The large efforts have resulted in series new compounds such as layered mixed transition metal (Ni-Mn-Co) oxides (e.g., $LiNi_{1/3}Co_{1/3}Mn_{1/3}O_2$) [3] and olivine lithium iron phosphate (e.g., $LiFePO_4$) [4], which appear to be promising cathode alternatives for $LiCoO_2$ and is in the stage of application. In the anode side, research remains more urgent, although various exotic carbonaceous and non-carbonaceous materials, e.g., disordered carbon [5], Li-alloys [6], lithium transition metal nitrides [7], transition metal oxides [8] and composite tin oxides [9], have been deeply studied with an improved capacity. It means that the "standard" carbonaceous materials, such as graphite and coke, are still likely to be the anode of choice for the next few years. A considerable investigation in our group for developing further Li-ion batteries has been under progress over 10 years and has lead to some remarkable results including of the electrode materials, the electrolytes and the battery system. In this paper, we give a brief introduction of the anode research of recent two years. Especially, the synthesis, characterization, electrochemical behavior and safety problem of these novel anode materials are discussed and presented in detail according to the types of electrolytes, such as liquid organic electrolytes and solid polymer electrolytes.

Long time

Part I: Liquid electrolytes based system

1. Li-alloy based composites

1.1 Introduction

The replacement of the Li metal anode by Li-alloys in rechargeable Li-ion cell has been under investigation since Dey demonstrated the possibility of electrochemical formation of Li_xAl in liquid organic electrolytes in 1971 [10]. Since that, it has been found that numerous metals, e.g., Mg, Ca, Al, Si, Ge, Sn, Pb, Sb, Bi, etc., can reversibly accommodate lithium under an electrochemical alloying process according to the mechanism: $xLi^+ + e^- + M = Li_xM$ [6]. Such a reaction can generate larger theoretic specific and volumetric capacities than the currently used lithiated graphite (LiC_6). In addition, the reactive potential of the lithium alloying process is close to that of the metallic lithium. Therefore, there has been a long time consideration for using Li-alloys as promising anode candidates for Li-ion cell. In general, Li-alloys have several advantages over carbonaceous materials which favor their use in a Li-ion cell, including of higher lithium storage capacities, in particular, when the charge densities are comparable to metallic lithium, and a relatively higher operating voltage, retarding the deposition of metallic lithium during charge, and thus improving safety and fast-charging capability. Besides, Li-alloys appear not to have much sensitive to the solvent co-intercalation compared with the graphitic anode materials. However, there is a major problem that encumbers the application of Li-alloys. This is mainly due to that the volume mismatch of the alloy hosts between Li intercalation and extraction are comparatively large (typically in the scale of over ca. 200 %), as shown in Fig.2, and such that the host matrix undergoes drastic mechanical stresses during charge and discharge. Such a mechanical degradation results in the metal cracks and the host particle pulverizes, and thus looses mechanical and electrical contact. Eventually, capacity fading is inevitable. By contrast, the dimensional stability of the carbonaceous host matrix during cycling is associated with very low volume changes during intercalation and removal of lithium (ca. 8%, for graphite) that results in good charge reversibility. There have been two major designs to overcome the pulverization dilemma of Li-alloys. One is based on the concept using composite or multiphase structure, in which the active material/phase is supported by the less-active or even non-active matrices, to keep the mechanical integrity [11].

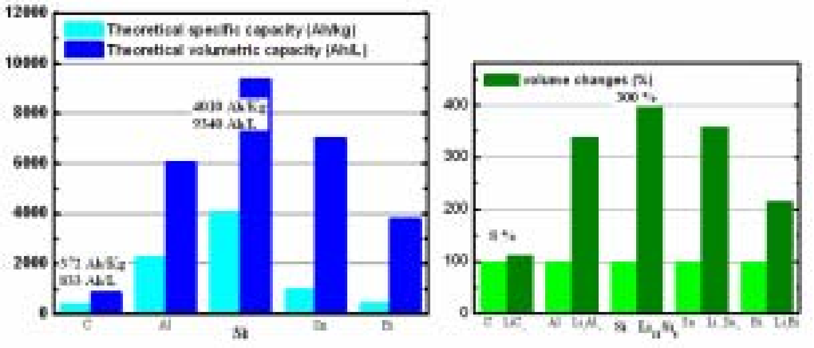

Fig.2 Capacity density and correspondingly volume changes before/after Li intercalation of different Li hosts.

The other approach is to suppress the drastic volume changes by designing a proper morphology of the hosts, characterized by thin layers comprising small particle size active material [12]. The effort to conquer the morphology instability of the Li-alloys leads to a challenge in the material research. Recently, we pay our attention on silicon, which has a low reactive potential of ca. 0.2 V vs. Li/Li^{-1} and has the highest capacity of ca. 4000 mAh g^{-1}, which is 10 times as that of the current graphite, among all known lithium storage hosts. [13-17]. However, similar to other Li-alloys, silicon possesses poor capacity retention during cycling due to the volume mismatch upon Li intercalation and extraction. As mentioned, a promising approach to overcome the volume effect is to create a composite microstructure comprising the active silicon uniformly dispersed in an inert matrix. The Sn-Fe-C nano-composites consisting of active $FeSn_2$ and inactive SnFeC proposed by Dahn' and co-workers suggest that high-energy mechanical milling (HEMM) could be an appropriate process to built such a composite microstructure [18]. By this way, some examples such as TiN-Si, TiB_2-Si, FeSi-graphite, and SiC-Si composites have been reported with the improved cyclability [19-22].

From an application standpoint, a considerable improvement in the first cycle efficiency and the cycling life remains to be done for such anode systems. There has been another attention that focuses on composites consisting of silicon and carbonaceous matrices. For instance, silicon covered with carbon by thermal vapor deposition (TVD) showed a better cycling stability than the pure silicon [23-25]. Dahn et al. reported that by pyrolyzing siloxane polymer or blends of pitch and polysine, silicon could be incorporated into carbon at atomic scale. These materials had a stable capacity of ca. 500 mAh g^{-1} but low initial faradaic yield [26, 27]. We also reported that pyrolysis of pitch or poly (vinyl chloride) (PVC) embedded with silicon and graphite provided an effective way to suppress the volume effects of silicon [28-32]. The enhanced cyclability is attributed to the small volume expansion of carbon on lithium intercalation (*ca.* 9% for graphite) and the ability of the ductile carbon to accommodate the volume change of silicon, reducing mechanical strain within the electrode and consequent electrode disintegration. Although this type of pyrolyzed carbon has a large potential hysteresis between Li-insertion and extraction, it may mostly function as an elastic network with electron/ion conductivity that permits the silicon in the carbon matrix to operate while maintaining electrode integrity. It seems that to a great extent the cycle performance of the pyrolyzed Si-C systems depends on the distribution of silicon and the contact strength between the active host and the matrix. However, a single pyrolysis step appears to be insufficient. We found that a combination of high-energy mechanical milling (HEMM) treatment with pyrolyzed process in the preparation for the Si-C composites can overcome the mentioned detriment from pyrolysis reaction and HEMM step alone. By this way, a series of Si-based composites have been proposed. The Si-C composite synthesized from two PVC pyrolysis reactions, combined with an intervening HEMM step, shows good cycling and large capacity of 900 mAh g^{-1}, plus high initial coulombic efficiency [28,29]. The Si-M-C composites prepared from ballmilling silicon with the inert conducting components and followed by a PVC pyrolysis process also show both good capacity and capacity retention [30-32]. In this part, characterization of the proposed Si based materials are presented and discussed in detail.

1.2. Experimental

1.2.1 Material preparations.

The basic preparation of the Si-C (silicon/disordered carbon) composite was as follows: poly (vinyl chloride) (PVC, Aldrich) and silicon particles (<1 μm, >99.8%) were homogeneously mixed and the weight ratio of silicon vs. PVC was 3:7. The mixture was heated at 900℃ in an Ar atmosphere for 1 h at a heating rate of 5 ℃ min^{-1} and allowed cool down to room temperature normally. The products were further treated by a high-energy mechanical milling (HEMM) step in a sealed bowl in Ar at a rotational speed of 500 rpm for 2-10 h. The resulting samples were mixed with PVC again (Milled product vs. PVC was 3:7, wt.%). The mixture was processed by a pyrolysis reaction following the same procedures as the first heating process. The preparation of the Si-M-C (M, a kind of co-ballmilling component; C, pyrolyzed PVC) composites was as follows: Si-M mixture consisting of silicon particles and TiN (ca. 1.5 μm), graphitic carbon (average particle size: 10-20 μm) with a weight ratio of 1:1 was treated by high-energy mechanical milling in a sealed bowl in Ar at a rotational speed of 500 rpm for 2-10 h. The resulting product was mixed with poly (vinyl chloride) (milled product vs. PVC was 3:7, wt. %) and heated at 900℃ in an Ar atmosphere for 1 h at heating rate of 5 ℃ min^{-1} and allowed cool down to room temperature normally. The final samples were ground and sieved. The $SiMg_2$ and $NiSi_2$ (Aldrich) materials were prepared by treating the commercially obtained products with HEMM and further sieved. Nano-size $SiO_{1.1}$ (typical particle size: 50 nm, prepared by CVD) was kindly grafted from Nagaku Ltd.co. Powder X-ray diffraction (XRD) patterns were obtained using automated powder diffractometer with Cu K_α radiation (Rotaflex RU-200B, Rigaku-denki Corporation). The morphology performance of the materials was characterized with scanning electron microscopy (SEM) and Electron Probe Micro-Analysis (EPMA).

1.2.3 Cell assembly and electrochemical tests.-

The electrode containing 8 wt% acetylene black (AB), 80 wt% active materials and 12 wt% Poly (vinylidene fluoride) (PVDF) was prepared by a normal casting. The active powders and AB were homogeneously mixed in a 0.02 g mL^{-1} PVDF/1-methyl-2-pyrrolidone (NMP) solution, and the vicious mixture was cast onto a 300-μm thick Ni foam, which served as a current collector. The electrode was further dried at 120℃ under vacuum for 2 h until NMP solvent was entirely removed. After pressing, the geometric area of the electrodes was 1.0 cm^2, and the typical thickness was 190~200 μm. To evaluate the electrochemical properties of the electrodes, a half-cell containing $LiClO_4$ / EC+DMC (Ethylene carbonate plus diethyl carbonate as 1:1 in volume) electrolyte was used, and lithium metal was utilized as the counter electrode. All the three layers, including test electrode, separator and lithium metal, were stacked in a 2025 coin type cell in a glove box. Unless stated elsewhere, cycling was carried out at a constant current density of 0.18 mA mg^{-1} and a voltage cutoff at 1.5/0.02V vs.Li/Li^+. Charge and discharge of the cell refer, respectively, to lithium extraction from, and insertion into, the active hosts. Electrode capacity was calculated according to the weight of active materials.

1.3 Results and discussion

1.3.1 Electrochemical behavior of pure Si insertion host

The electrochemical characterization of the silicon with different particle size was investigated and compared in Fig.3. All the silicon is reactive to lithium that results in a large capacity. A decrease in the particle size enhanced the solid electrolyte interface (SEI) film formation on the surface of the active hosts; thereby it increased the capacity loss in the first cycle. There is an obvious shift in the discharge potential plateau from the first cycle to the second cycle that could relate to the irreversible phase transformation of silicon from crystalline to amorphous state in the first electrochemical alloying process. Capacity retention shows high similarity for the silicon with different particle size, indicating that the morphology deteriorating mechanism of Si upon charge and discharge is obviously dissimilar from normal alloy hosts, such as Sn, whose cyclability is highly dependent on the particle size, as mentioned in the introduction part. Fig.4 shows such an imaginable mechanism difference in the morphology changes upon Li insertion and extraction for Si (a) and Sn (b) based hosts. Differing form that of Sn, the repeated Li insertion into and extraction from the active Si do not cause a particle collapse. By contrast, the volume expansion and shrink of Si possess homogeneous change due to the electrochemical driven

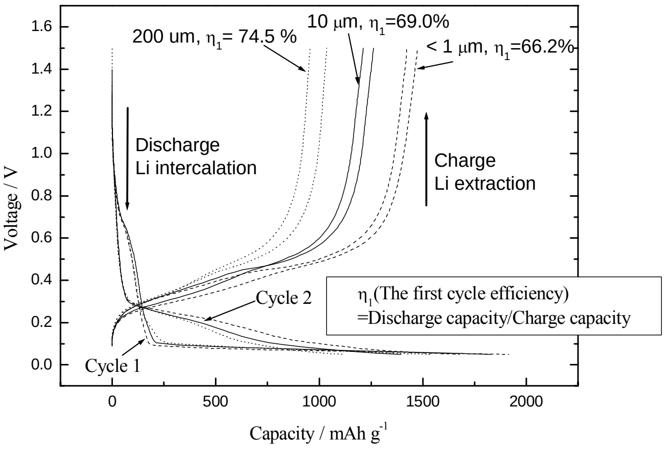

Fig.3. Charge and discharge profiles of the silicon with different particle size.

amorphous character. However, the volume effects inevitably result in electron-contacting loss in both Si and Sn, and finally cause capacity fading. A further understanding with respect to the morphology failure mechanism of Si is still in the progress.

1.3.2 High mechanical stable Si-C composites for Li intercalation

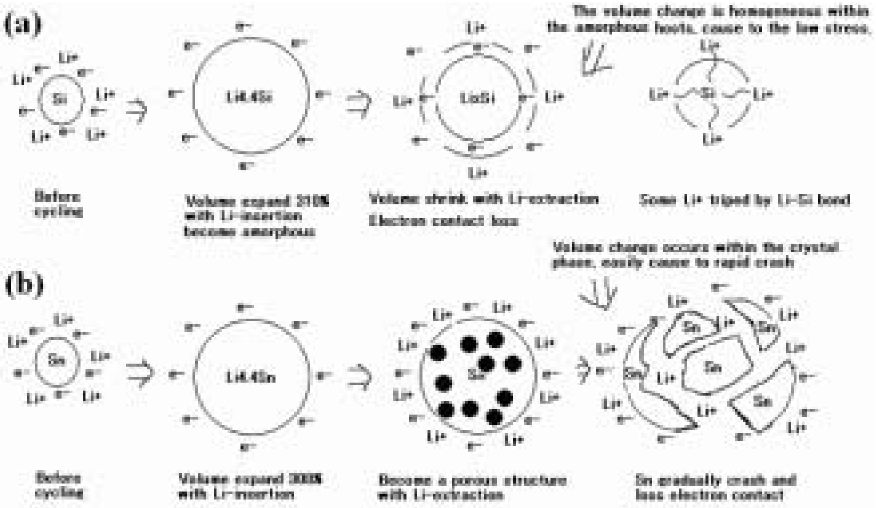

Fig.4. Mechanism of morphology changes of Si and Sn Li upon Li intercalation and extraction.

To suppress the volume effects of silicon upon cycling, we try to disperse ultrafine silicon into a feasible carbonaceous matrix by means of pyrolyzed PVC reaction and HEMM process. The inset in Fig.5 shows charge and discharge profiles of the Si-C electrode at different cycles. Insertion potential of silicon in the first cycle mainly occurs below 0.1V, yielding an extremely flat plateau. The average potentials of the composite in the discharge and charge stage are 0.2 V and 0.4 V. The electrochemical behavior of the composite is dominated by silicon insertion host, suggesting only small amount lithium storages in the carbonaceous matrix. The faradaic yield of extraction to insertion is close to 100 % after the second cycle, versus 82.6% at the first cycle.

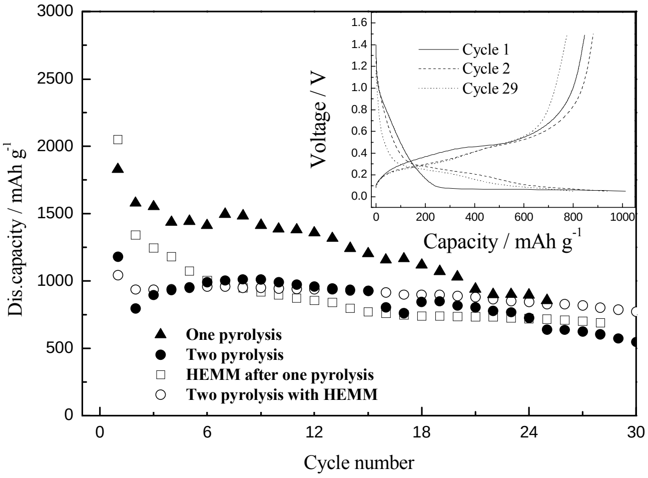

Fig.5 Cycling performance of the Si-based composites prepared from different procedure. The inset figure is charge and discharge profiles of the Si-C composite.

The synthesis steps have obvious effects upon the electrochemical behavior of the composites. Fig.5 illustrates the cycling performance of the Si-C composite prepared from different procedures. One pyrolysis reaction has the worst capacity retention. SEM analysis reveals that the Si-distribution, as shown in Fig.6a, is relatively poor. Some cracks and lots of silicon over the surface of the composite suggest the unstable morphology and incompletely embedding can hardly prevent Si from deterioration. The composite synthesized from two pyrolysis processes without HEMM step has a slightly improvement in the cycling performance. By contrast, HEMM appears to be highly favorable for long cyclability. HEMM is well known as an effective energy transfer way via the vigorously interfacial collisions among precursors and balls. It

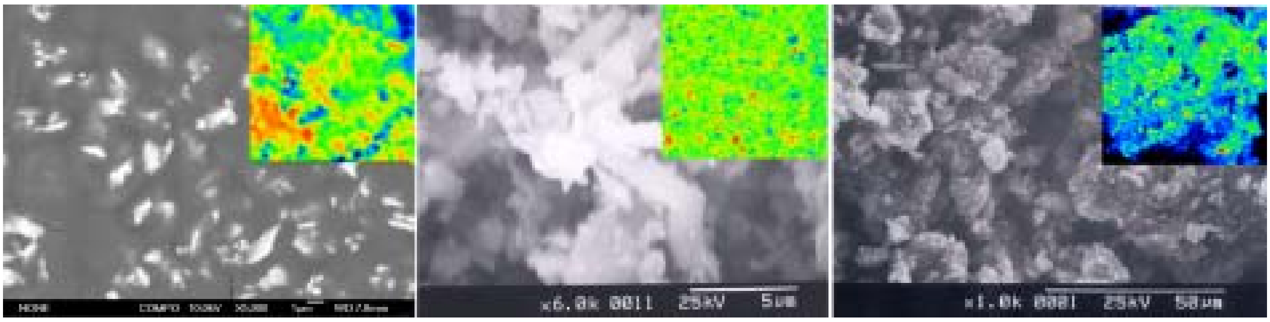

Fig.6 SEM and corresponding EPMA images of the composites prepared from a) one pyrolysis reaction; b) after one pyrolysis reaction and HEMM; and c) two pyrolysis reaction with a an intervening HEMM step.

enhances Si/C contact and generates many Si-C clusters with a multiphase structure formed under the strong particle impacts, as shown in Fig.6b. Such a structure can achieve the reasonably improved interface affinity between the silicon and the carbonaceous matrix. HEMM also increases the packing density by reducing the porosity of the pyrolyzed PVC from the first pyrolysis, and ensures the adherent integrity between the dispersed silicon and the carbonaceous matrix. However, HEMM increase the initial irreversible capacity due to an enhanced SEI formation on the surface of the particles. The composite made from HEMM step between two pyrolysis reactions possesses the best cycling. The corresponding EPMA analysis reveal that no obvious silicon regions could be identified, implying that the silicon particles are completely embedded in the disordered carbon. The large particle of the composite also leads to a reasonable initial coulombic efficiency, as shown in Fig.6c.

A favorable structure concerning this type of composite is that silicon is completely and uniformly trapped and embedded in the carbonaceous matrix. We believe that the key points determining the mechanical stability are homogeneous Si-distribution and high adhesion strength between the silicon and the matrix. By this way, a possible aggregation of silicon can be highly avoided and a good electron-contacting channel can always be maintained. A comparison with pure silicon in the cycling performance reveals that the Si-C composite has a remarkably enhanced cyclability, as shown in Fig.7. Controlling Li-insertion level at 600 mAh g^{-1} can effectively improve the morphology stability of the composite electrode. This can be explained by the alleviated electrode disintegration and deactivation. Reducing the Li-insertion degree suppresses electrode degradation on cycling.

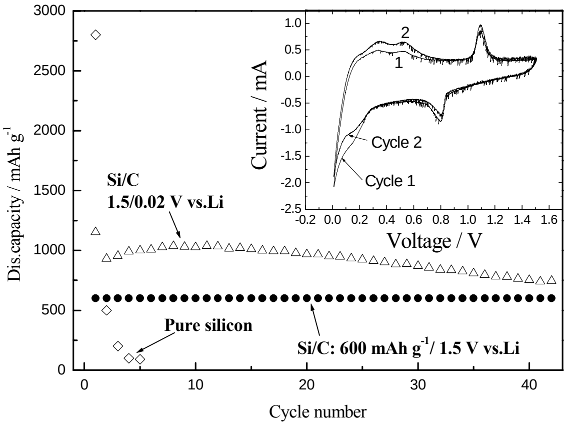

Fig.7. Cycling performance of the Si-M-C composites based electrodes. The inset figure is CV profiles of the Si-C composite prepared at 1000 °C.

The synthesis temperature has an obvious effect upon the electrochemical behavior of the samples. The inset in Fig.7 illustrates the CV curves of the 1000°C product. There are three cathodic peaks appear during the Li-insertion process at the first cycle: 0.8V, 0.15 V and 0.01V. The latter two peaks mainly link to Li-intercalation into disordered carbon and silicon respectively. The former one, however, could be due to a new compound formed under the prolysis reaction. Also during the anodic scan, three peaks can be found at 0.3 V, 0.55 V and 1.1 V, representing three Li-extraction stages which correspond to silicon, disordered carbon and the new compound. The 0.8V cathodic peak and the 1.1V anodic peak display the high reversibility.

1.3.3 The introducing of relatively inert components in the Si-C composites

Fig.8 shows X-ray diffraction patterns of the resulting powders of a) Si-C, b) Si-graphite-C and c) Si-TiN-C composites. All the composites indicate the presence of crystalline silicon. Especially, the peak reflection of silicon in the Si-C composite is remarkable, suggesting that HEMM may have a weak influence upon the crystallite of silicon. By contrast, it is characteristic that intensity decreasing and peak broadening reflected from silicon in the Si-TiN-C composites are noticeable compared with those in the Si-graphite-C and Si-C composites. This is probably attributed to that the relatively hard TiN tends to reduce the crystallite size of silicon and make the active particles partly amorphous during the HEMM treatment.

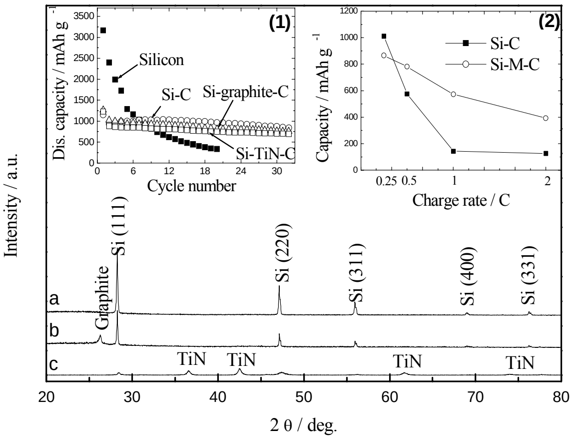

Fig.8. XRD patterns of the resulting composites of a) Si-C, b) Si-graphite-C and c) Si-TiN-C. The inset figure (1) is cycling performance of different composites and inset figure (2) is Charging rate as a function upon the reversible capacity of the Si-C and Si-M-C composites.

All the composites have a high similarity in the voltage trends upon charge and discharge. The cycling performance of the Si-based composites was shown in the inset (1) in Fig.8. The composites have a remarkably enhancement in the morphology stability for Li insertion. As mentioned, there are several possibilities for such a cycling improvement. First, HEMM increases the Si-distribution and decreases the active particle size. Secondly, the improved adhesion strength between the silicon and the relatively inert components treated under HEMM can hold a good electron-contacting. Finally, pyrolyzed PVC can cover the milled Si-clusters and function as an elastic network with electron/ion conductivity that permits the silicon in the carbon matrix to operate while maintaining electrode integrity. The pyrolyzed PVC also can function as a binder to hold the mechanical integrity among different components. Due to the poor electron-conductivity of silicon in the origin, the Si-C composite suffers from an obvious loss in the reversible capacity with increasing the charging rate, as shown in the inset (2) in Fig.8. In the case of the Si-M-C composites, the reversible capacity can be remained to be ca. 50%, when the charging rate was increased to 2C. A decreased particle size of the silicon active hosts may take this consequence. It means that ballmilling silicon with the conducting TiN and graphite prior to the pyrolysis reaction tends to decrease the active particles size and brings an obviously improvement in the charging rate over the Si-C composite. However, silicon suffers from a loss in the capacity utilization due to an inactive phase formed between the silicon and the co-milling components. Especially, the milling time is extended.

1.3.4 Comparison in the cycling stability of different Si hosts materials

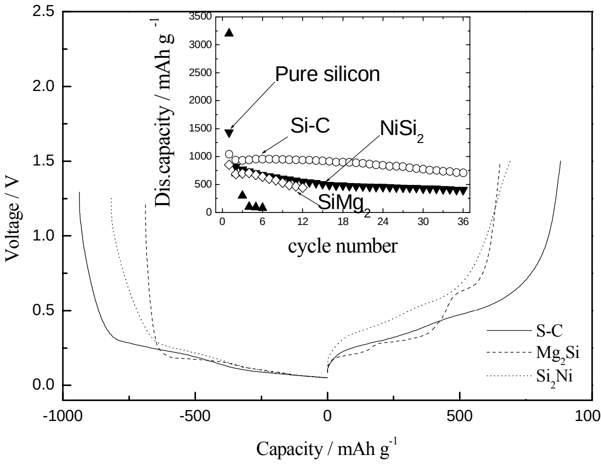

Fig.9. Charge and discharge profiles of different silicon based hosts. The inset figure is cycling performance of different silicon based hosts.

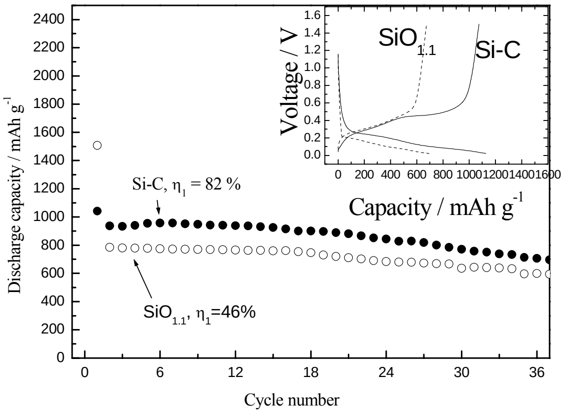

Fig.10. Cycling performance of different silicon based hosts. The inset figure is charge and discharge profiles of different silicon based hosts.

Adopting intermetallic multiphase structure also can apparently alleviate the morphology instability of silicon for Li-insertion. Fig.9 shows the charge and discharge curves of the electrodes based on $NiSi_2$, $SiMg_2$ and Si-C composite at the second cycle. Two obvious discharge potential plateaus at 0.2V and 0.1V of the $SiMg_2$ electrode is linked to Li-intercalation process to form a single crystalline $LiMg_2Si$, following a reaction between Li and Si, finally lithium may alloy with Mg. Also, two charge potential plateaus appear at 0.3 V and 0.7 V, representing the Li-extraction stage that reveres to the Li-Si-Mg alloy process. In the case of $NiSi_2$ and Si-C composite, similar electrochemical behaviors suggest that the insertion mechanism of both hosts is only related to the electrochemical Li-Si alloying reaction. Although silicon content in Si_2Ni (*ca.*48 wt %) is almost equal to that of the silicon/disordered carbon composite, the latter shows much larger reversible capacity, indicating the higher electrochemical reactivity. The cycling performance of the electrodes based on pure silicon, $NiSi_2$, $SiMg_2$ and silicon/disordered carbon composite is shown in the inset in Fig.9. All the composite shows the relatively improved cycling stability compared to pure silicon. However, due to the comparable "crash" characteristic of the metallic matrix, the mechanical stability of $NiSi_2$ and $SiMg_2$ is obviously inferior to the silicon/disordered carbon composite. Especially in the case of $SiMg_2$, a close reactive potential scale of Mg and Si will easily cause to a rapid capacity decline, suggesting that the Li-Si-Mg process is only partially reversible. Oxide such as inert Li_2O and SiO_2 also play a noticeable effect to enhance the morphology stability of silicon upon volume change. X-ray diffraction patterns reveal that the single phase of intermetallic $NiSi_2$ and $SiMg_2$ can be recognized. By contrast, the relatively weak peak indicates that $SiO_{1.1}$ contains lot of amorphous SiO and SiO_2 besides crystalline silicon. The inset in Fig.10 shows the comparison of the charge and discharge behaviors between $SiO_{1.1}$ and Si-C. The discharge plateau of $SiO_{1.1}$ is slightly lower than that of silicon/disordered carbon, indicating Si and SiO_2 within the $SiO_{1.1}$ electrode may be obstructive to the initial Li-insertion. Cycling performance of the electrodes based on $SiO_{1.1}$ and Si-C composite is shown in the inset in Fig.10. A significantly initial capacity loss of the $SiO_{1.1}$

electrode can be noticed, relating to an irreversible reaction of amorphous SiO with lithium to form Li_2O and Si at the first cycle. The huge specific area of nanosize active hosts also takes part consequence. Due to buffering effect of Li_2O and SiO_2, the high capacity retention is also remarkable for $SiO_{1.1}$. Bear in mind that a noticeably large irreversible capacity loss of $SiO_{1.1}$ in the first cycle is inevitable; the electrochemical performance of the Si-C composite is obviously superior to that of $SiO_{1.1}$.

1.3.5 Thermal stability of the Si-C based composites under lithiated state

It is well known that the thermal stability of the graphite anode in the inorganic electrolytes is controlled by the SEI film formed on the surface of the lithiated active hosts [35]. Since the reactive potential of the composite is close to that of graphite after the first cycle and the SEI film is formed on the surface of the carbonaceous matrix, it is reasonable that the thermal behavior of the Si-C under lithiated state is similar to graphite, as shown in Fig.11. There are two sharp exothermic peaks and a small one starting from 130°C to 280°C for the graphite electrode, which correspond to a mild heat generation caused by the reaction (SEI formation) of the electrolytes and the lithiated graphite. The exothermic peak at 280 °C is probably due to the reaction of lithiated graphite and electrolytes by a breakdown of the SEI as reported by J.R.Dahn et al. and J.Yamaki et al [35, 36]. However, the matched exothermic peak at 280°C of the Si-C composite significantly turns into weak, indicating a relatively low heating generation due to the comparatively increased insertion potential. Moreover, the lithium storage in disordered carbon is extremely lower than that of silicon. The later, on the other hand, is embedded inside and a direct contact with electrolytes is highly avoided. It also leads to the relatively improved thermal stability.

1.3.6 High energy density Li-ion cells consisting of silicon based anodes

A comparison with mesocarbon microbead (MCMB, a kind of commercial graphitic carbon) in the charge and discharge profiles at the second cycle reveals that the Si-based composite has a slight increase in the Li insertion and extraction potential plateau for about 0.12 V, as shown in inset (b) in Fig.11. This, in turn, can prevent lithium dendrite formation at a high charging rate and leads to an enhanced operation safety. However, the Si-based composite surfers from a loss in the volume capacity due to a low density (1.7 g cm^{-3}, in case of Si-C) compared with that of MCMB (ca. 2.25 g cm^{-3}). A full cell using the Si-C composite anode and the $LiNi_{0.8}Co_{0.2}O_2$ cathode was fabricated to study its electrochemical characteristics, as shown in the inset (a) in Fig.11. For full utilization of lithium storage capacity of the Si-C composite anode, the weight of cathode has to be much over that of the anode (7−8 times). The cell has a large anode capacity of ca. 600 mAh g^{-1} within the working potential of 2.3−3.9 V that might result in high energy density.

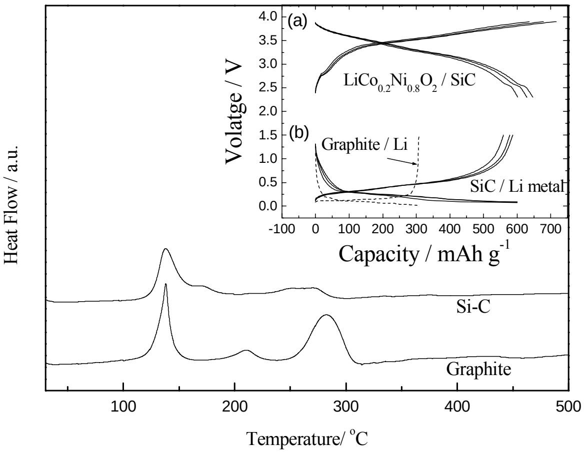

Fig.11. The DSC curves of silicon/disordered carbon composite and graphite under lithiated state. Scan rate: 5 **°C** min^{-1} under Ar flow of 100ml min^{-1}. The inset figure is the charge and discharge profiles of different cells.

1.4 Conclusion

The volume effects of silicon upon Li insertion and extraction can be effectively suppressed by designing a composite microstructure containing that ultrafine silicon are uniformly dispersed in a ductile conducting carbonaceous matrix with electron/ion conductivity. By this way, several types of Si-based composites have been developed by means of pyrolysis process in accompany with high-energy mechanical milling step. The pyrolyzed carbon can mostly function as an elastic network with electron/ion conductivity that permits the silicon in the matrix to operate while maintaining electrode integrity. The Si-based composites have large capacity of ca. 1000 mAh g^{-1} and good cycling performance, as well as acceptable first cycle efficiency. We expect that further optimization of these Si-composite based anodes might lead to practical lithium-ion batteries with high energy density.

2. Lithium transition metal nitrides based composite electrodes

2.1 Introduction

In view of the morphology stability, especially, under high Li-utilization, lithium transition metal nitrides with hexagonal symmetry, P6/*mmm*, such as $Li_{2.6}M_{0.4}N$ (M=Co, Cu, Ni), are superior to Li-alloy in the cyclability as promising anode candidates. The ternary $Li_{2.6}Co_{0.4}N$ is composed of Co substituting lithium between the $Li_2^+N^{3-}$ layers of Li_3N. Li_3N has two kinds of Li ion. That is, location (1): Li ion is located in the Li_2N layer and (2): Li ion is located between the Li_2N layers. It is believed that Co substitutes Li ion in the location (2), as shown in Fig.12. The intercalation mechanism of the layered lithium transition metal nitrides has been primarily investigated by this group and T. Shodai et al. [7,37-40]. The solid solution range of the $Li_{3-x}M_xN$ is located in $0<x<0.5$, $0<x<0.6$ and $0<x<0.3$ for M=Co, Ni and Cu correspondingly. From an electrochemical standpoint, the most promising and most studied of the compound in this family is $Li_{2.6}Co_{0.4}N$. It was found that the large capacity of 900 mAh g^{-1} of $Li_{2.6}Co_{0.4}N$ is associated with a structure change from a crystal to an amorphous phase in the first Li-extraction process [41]. Such a transformation indicates the atom rearrangement and lithium in the compounds can be electrochemically extracted and re-intercalated with high reversibility. However, $Li_{2.6}Co_{0.4}N$ does not show satisfactory capacity retention upon long cycles. The capacity fading is attributed to the electrochemical instability under high Li-extraction and the interfacial incomparability on the surface of the active hosts [42,43]. In the pervious work, we have developed a series co-doped lithium transition metal nitrides by means of combination of solid-state reaction at high temperature and high-energy mechanical milling (HEMM) process [44]. These compounds are superior to ternary $Li_{2.6}Co_{0.4}N$ in terms of capacity retention and cost. On the other hand, lithium must be extracted from the nitrides in an initial anodic oxidation, indicating that these Li-rich type anodes cannot directly combine with the typical high potential cathodes such as $LiCoO_2$ and $LiMn_2O_4$ to make Li-ion cells. We have showed that the Li-rich compounds can be used as insertion hosts in several ways. For example, lithium in the compounds can be pre-extracted by a chemical way before assembling a cell [45]. Lithium metal nitrides also can be introduced to make compensation for the irreversible capacities of the alloy, carbon and metal oxides based electrodes in the first cycle [46-48]. Furthermore, we designed a type of Si-graphite-$Li_{2.6}Co_{0.4}N$ composite via two HEMM steps [49]. Due to the capacity compensation from the lithiated $Li_{2.6}Co_{0.4}N$ in the first cycle, the composite material demonstrates an extremely high initial faradaic yield of 92%, as well as a large capacity and an acceptable cyclability. Recently, we have reported a composite electrode consisting of spinel $LiTi_2O_4$ and lithium metal nitrides. $LiTi_2O_4$ can extract lithium from the lithium transition metal nitrides and function as an inert-conducting material in the electrodes within a special potential range [50]. The composite electrode shows high volumetric capacity and excellent cycling stability. More recently, we found that the novel composite anodes, which consist of transition metal oxide, such as Co_3O_4, and hexagonal lithium transition metal nitrides, demonstrate high electrochemical capacities of about 500 mAh g^{-1} and 100 % capacity retention at the first cycle, as well as good cyclability [51]. Transition oxides can thermodynamically extract lithium from the lithium transition meal nitrides that leads to a delithated state of the nitrides and to form metallic Co and Li_2O. Thus, lithium transition metal nitrides can be directly treated as being in a delithiated state. Such a composite anode also shows high interfacial compatibility and low reaction heating with solid PEO electrolytes. In this part, some of the above obtained results based on the hexagonal lithium transition metal nitrides are presented and discussed in detail.

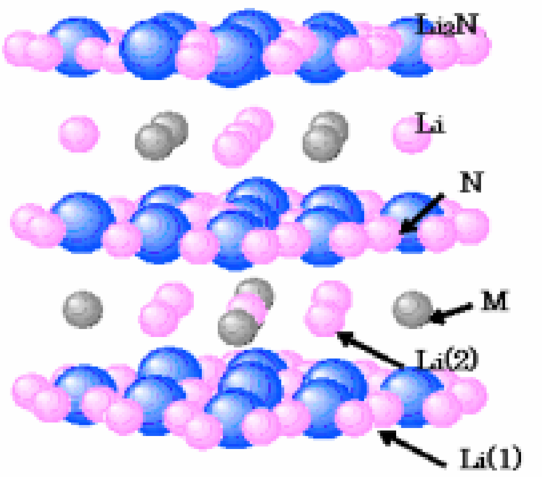

Fig.12. Structure model of the $Li_{2.6}Co_{0.4}N$.

2.2 Experimental

2.2.1 Materials preparations and XRD measurements

The hexagonal compound was prepared by a solid state reaction following a pervious report [7]. The basic procedure was as follows: mixtures of Li_3N and powders of transition metal were pressed into tablets with 8 mm in diameter and 5-8 mm in thickness in an Ar atmosphere. The tablets were heated at 700℃ for 12 h under a N_2 stream at a heating rate of 35 ℃ min^{-1}. The reactions were allowed cool down to room temperature normally. For the compounds containing Fe, heating temperature was increased to 800 ℃. The resulting products were ground in a glove box and further treated by high-energy mechanical milling (HEMM) at a rotational speed of 500 rpm for 20 h. Powder X-ray diffraction (XRD) patterns were obtained using automated powder diffractometer with Cu K_α radiation (Rotaflex RU-200B, Rigaku-denki Corporation). The samples assembling and measurements were performed under air-sealing condition.

2.2.2 Electrode fabrications and electrochemical measurements

A given weight of the electrode components, including 20 wt% acetylene black (AB), 70 wt% active materials and 10 wt% Poly (vinylidene fluoride) (PVDF), was homogeneously mixed in an agate mortar in a glove box and further pressed onto a 300-mesh stainless steel grid, which served as a current collector. The geometric area of the electrodes was 0.55 cm^2, and the typical thickness was 100~160 μm. Electrode capacity was calculated according to the weight of active materials. To evaluate the electrochemical properties of the electrode, a half-cell containing $LiPF_6$ / EC+DMC (Ethylene carbonate plus diethyl carbonate as 1:1 in volume) electrolytes was used. Li metal was utilized as both the counter and reference electrode. The structure of such a cell is similar to that of Si based cells. Basically, all the three layers, including test electrode, separator and Li metal, were stacked in a 2025 coin type cell in a glove box. Unless stated elsewhere, cycling was started from discharge and carried out at a potential cutoff at 1.4/0.01 V and a constant current density of 0.15 mA cm^{-2}. The rest time between charge and discharge was 1 min. Charge and discharge of the cell refer, respectively, to lithium extraction from, and insertion into, the active hosts. The impedance response was measured with a Solartron SI 1260 (impedance / gain-phase analyzer) in a frequency range from 0.1 to 10^6 Hz.

2.3 Results and discussion

2.3.1 The doped elementals upon the electrochemical behavior of the ternary $Li_{2.6}Co_{0.4}N$

The composition of the resulting compounds is confirmed by Inductively Coupled Plasma (ICP). Fig.13 shows X-ray diffraction patterns of the prepared lithium transition metal nitrides. The XRD responses are well in accordance with those of $Li_{2.6}Co_{0.4}N$ recorded on JCPDS card 5-605, indicating a typical hexagonal structure, isostructural with Li_3N, in which part of lithium in Li_3N is substituted by Co, Cu, Ni or Fe. No impurity phase, such as Li_2O, residual Li_3N and metals, can be detected. The collected lattice parameters of the hexagonal compounds are shown in the inset in Fig.13. Due to the atom radius of the doped metals, *e.g.*, Ni<Co<Cu, the a-axis gradually decreases from $Li_{2.6}Ni_{0.4}N$ to $Li_{2.6}Co_{0.4}N$, until $Li_{2.6}Cu_{0.4}N$. As a result, the affinity between the Li-M (M=Cu, Co, Ni) layer (2) and the Li^{1+}-N^{3}-Li^{+} layer (1) is decreased with the increasing of the affinity within the Li^{1+}-N^{3}-Li^{+} layers (1). The a-axis increases again in the range from $Li_{2.6}Cu_{0.4}N$ to $Li_{2.6}Ni_{0.4}N$. The c-axis is changed along with the opposite direction of a-axis. When Co content is 0.2, both a and c axis show the largest value in the case of Co, Cu and Ni coexist.

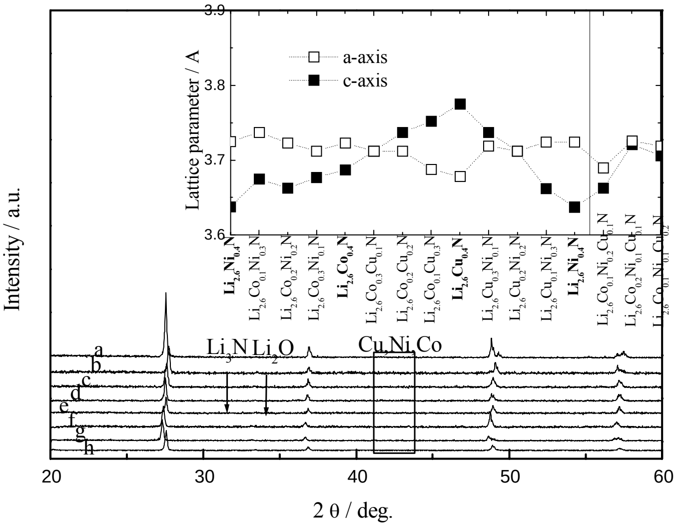

Fig.13. XRD patterns of the hexagonal lithium metal nitrides: a) $Li_{2.6}Co_{0.4}N$; b) $Li_{2.6}Co_{0.2}Cu_{0.2}N$; c) $Li_{2.6}Co_{0.2}Ni_{0.2}N$; d) $Li_{2.6}Cu_{0.2}Ni_{0.2}N$; e) $Li_{2.6}Co_{0.25}Cu_{0.15}N$; f) $Li_{2.6}Co_{0.2}Cu_{0.1}Ni_{0.1}N$; g) $Li_{2.6}Co_{0.25}Cu_{0.1}Ni_{0.05}N$; h)$Li_{2.6}Co_{0.2}Cu_{0.15}Fe_{0.05}N$. The inset figure is Lattice parameters of the lithium metal nitrides.

As found, the electrochemical behavior of the $Li_{2.6}Co_{0.4}N$ is superior to those of $Li_{2.6}Ni_{0.4}N$ and $Li_{2.6}Cu_{0.4}N$. To keep the charge balance of $Li_{2.6}Co_{0.4}N$ upon oxidation and reduction state, both cobalt and nitrogen play an important role. Fig.14 shows charge and discharge curves of the selected 1) $Li_{2.6}Co_{0.4}N$, 2) $Li_{2.6}Co_{0.2}Cu_{0.2}N$, 3) $Li_{2.6}Co_{0.2}Cu_{0.1}Ni_{0.1}N$ and 4) $Li_{2.6}Co_{0.2}Cu_{0.15}Fe_{0.05}N$ electrodes at different cycle. Due to the vacant sites introduced by the existence of Co^{2+}, the fully lithiated nitrides still permit small amount of lithium intercalation into in the first cycle, as shown in Fig.14a. The compounds gradually undergo an irreversible transformation from a crystal to an amorphous phase in the initial Li-extraction stage, resulting in the noticeable potential plateaus at 1.0, 1.2, 1.1 and 1.1 V for $Li_{2.6}Co_{0.4}N$, $Li_{2.6}Co_{0.2}Cu_{0.2}N$, $Li_{2.6}Co_{0.2}Cu_{0.1}Ni_{0.1}N$ and $Li_{2.6}Co_{0.2}Cu_{0.15}Fe_{0.05}N$, respectively. Compared with $Li_{2.6}Co_{0.4}N$, the obvious increases of $Li_{2.6}Co_{0.2}Cu_{0.2}N$, $Li_{2.6}Co_{0.2}Cu_{0.1}Ni_{0.1}N$ and $Li_{2.6}Co_{0.2}Cu_{0.15}Fe_{0.05}N$ in the charge potentials indicate that part Co substituted by Cu, Ni and Fe may be obstructive to the lithium extraction. At the fifth cycle, the $Li_{2.6}Co_{0.4}N$ and $Li_{2.6}Co_{0.2}Cu_{0.15}Fe_{0.05}N$ electrodes as shown in Fig.14b have a small potential fluctuation at *ca.*0.9 V and 1.3 V in the Li-extraction stage. This consequence is related to an atom rearrangement associated with the doped elementals, Li and N.

Cycling comparison reveals that the co-doped compounds have a remarkably enhanced cyclability, as shown in Fig.15. By optimizing the tradeoffs for capacity and cycling in accordance with the ternary $Li_{2.6}M_{0.4}N$, we have confirmed that the appropriate compositions in this family should be in the range, which can be stated by a formula as $Li_{2.6}Co_{0.4-x-y}Cu_xNi_yN$ ($0.1 \leq x \leq 0.2$, $0 \leq y \leq 0.1$, $0.1 \leq x+y \leq 0.2$). Furthermore, a certain amount of doped Fe was found to increase the capacity and is in favor for the cycling. Compared to $Li_{2.6}Co_{0.4}N$, the obviously improved cyclability of the co-doped compound may be partly attributed to the enhanced interfacial compatibility between the active particles and the electrolytes. The inset in Fig.15 shows Cole-Cole plots of the impedance response of $Li_{2.6}Co_{0.4}N$ and $Li_{2.6}Co_{0.2}Cu_{0.2}N$ electrodes with the delithiated stage vs. Li after 30 cycles. With part Co substituted by Cu, the total resistances of the half cell significantly turn into lessen, resulting in not only an improved interfacial compatibility, but also an enhanced capacity retention. In addition, according to the capacity utilization in $Li_{2.6}Co_{0.4}N$ and $Li_{2.6}Co_{0.2}Cu_{0.2}N$, the comparatively low Li-extraction level in $Li_{2.6}Co_{0.2}Cu_{0.2}N$ is favorable for the cycling stability. We have observed that the capacity fading of the ternary $Li_{2.6-z}Co_{0.4}N$ can be effectively suppressed if the Li-extraction is limited at $z \leq 1.0$.

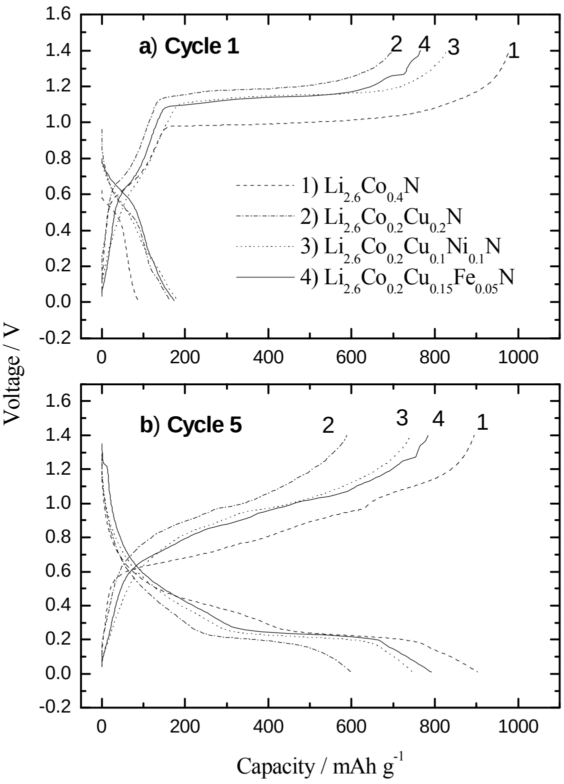

Fig.14. Charge and discharge profiles of the lithium metal nitrides electrodes at a) cycle 1 and b) cycle 5.

To further unveil the reliance of the electrochemical behavior upon the structure change along with Li-extraction, the variation of the lattice parameters of $Li_{2.6-Z}Co_{0.4}N$ and $Li_{2.6-Z}Co_{0.2}Cu_{0.2}N$ with various charge-discharge depths in the scale of $0<Z<1.0$ in the first Li-insertion/extraction process was measured and shown in Fig.16. The pointed sites of a~e in a_1 and b_1 indicate the special Li-insertion/extraction stage while the corresponding lattice parameters are shown in a_2 and b_2. In the charge process, it is obvious that the a-axis decreases with the c-axis increases, relating to the composition range where the potential gradually increases to 1.0 V for $Li_{2.6}Co_{0.4}N$. Above z~0.3, no remarkable change in the cell parameter is observed until z=1.0, but decline in the XRD responses peak turn into noticeable. It suggests that the Li-extraction is associated with the two-phase reaction and the crystalline structure finally becomes amorphous. In the case of $Li_{2.6-Z}Co_{0.2}Cu_{0.2}N$, the slight decreasing of a-axis along with the increasing of c-axis occurs much early, and there is no change in the lattice parameter above z~0.2. However, we notice that the crystalline response peaks, which are linked to the phase transformation, apparently reduce. It indicates that the formation of an amorphous phase appears in the very early charge region. As a result, lithium extraction from the $Li_{2.6-Z}Co_{0.2}Cu_{0.2}N$ becomes difficult, leading to a decreased capacity compared to that of the $Li_{2.6-z}Co_{0.4}N$.

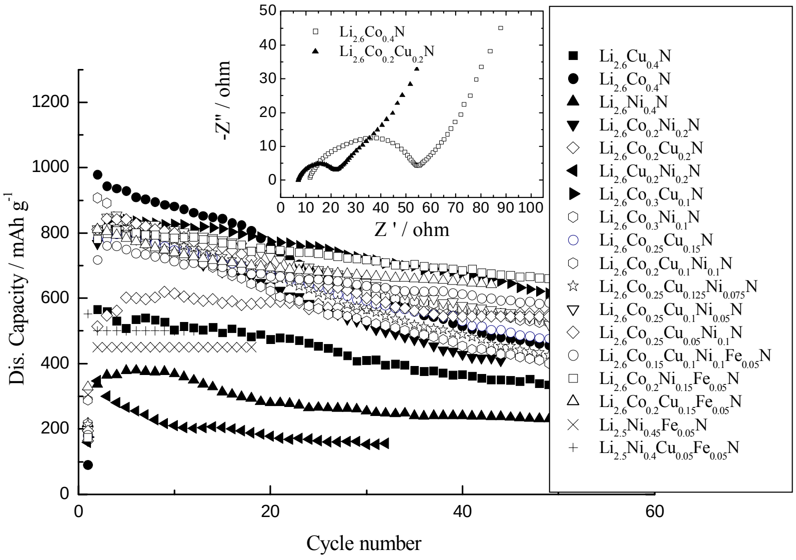

Fig.15. Cycling performance of the lithium metal nitrides electrodes. The inset figure is Cole-Cole plots of the impedance response of the a) $Li_{2.6}Co_{0.4}N$ and b) $Li_{2.6}Co_{0.2}Cu_{0.2}N$ with the charged state after 30 cycles.

2.3.2 The effects of the morphology performance upon the electrochemical behavior

Morphology performance of the particles after was found to show obvious effects upon the electrochemical behavior. Fig.17 shows charge and discharge curves of $Li_{2.6}Co_{0.2}Cu_{0.2}N$ without and with HEMM. The initial insertion capacities were significantly enlarged when the particles were treated under HEMM for 20h. Compared with the un-milled samples, the milled nitrides had an obviously decreased ratio of Li vs. doped elementals from the ICP measurements. It appears to be related to the increased Li-free sites and the valance change of part Co. Thus, we assumed that HEMM enables the removal of part lithium in the Li-rich compounds. A decrease in the first extraction potential plateau probably is attributed to that HEMM make the crystalline lithium transition metal nitrides partly amorphous. The milled samples have an increased capacity and a decreased Li-extraction potential. This can be explained by the reduced potential polarization arising from the improved electrochemical kinetics, e.g., the shorten lithium diffusion path and the improved interfacial charge transfer that relates to the enlarged reactive area of the insertion hosts. The HEMM alleviates the obstruction to the lithium extraction; thereby increases the Li-extraction degree at a certain extent. A comparable cycling stability of the milled lithium transition metal nitrides is available in accompany with a deep Li-extraction, as shown in the inset in Fig.17. However, the $Li_{2.6}Co_{0.2}Cu_{0.2}N$ directly synthesized by HEMM does not bring the same consequence. It is probably due to the incomplete reaction and poor atom distribution. We have observed a lot of residual Li_3N and transition metals in the XRD patterns for the sample prepared by HEMM. This means that high-energy mechanical milling step alone is insufficient for achieving the good crystalline formation for the multi-doped compounds.

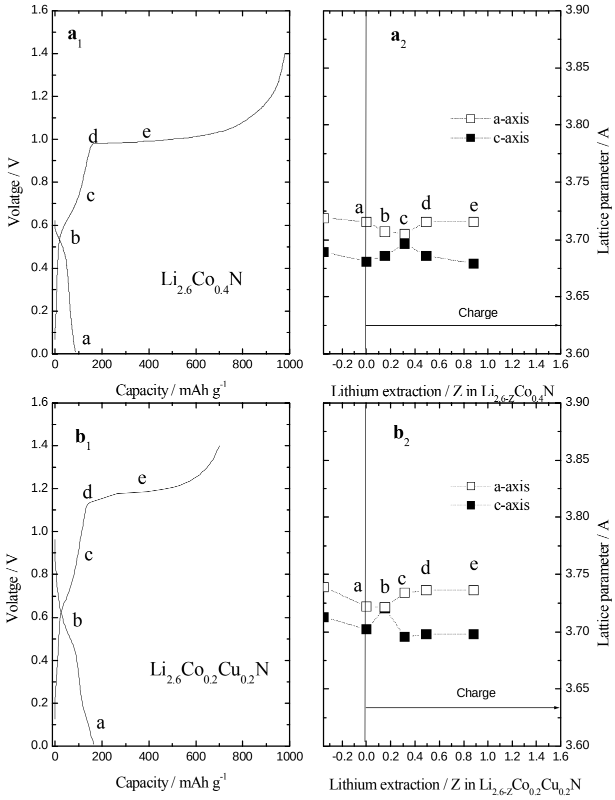

Fig.16. Variation of lattice parameters of the a) $Li_{2.6}Co_{0.4}N$ and b) $Li_{2.6}Co_{0.2}Cu_{0.2}N$ with various Li-insertion/extraction depths in the first cycle.

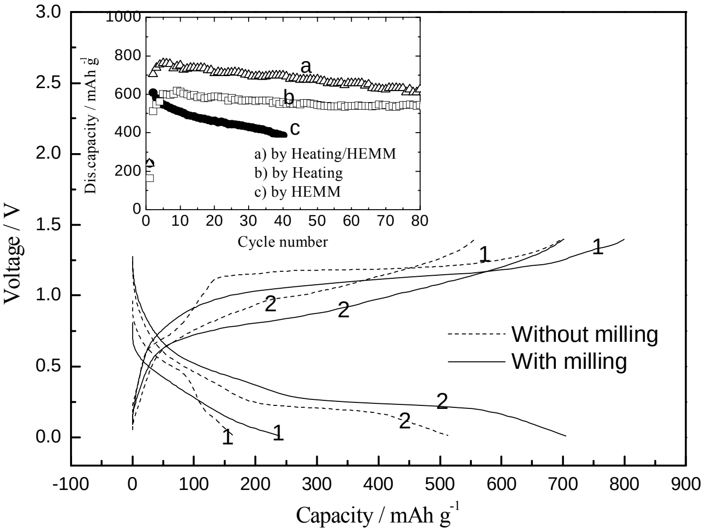

Fig.17. Charge and discharge curves of the electrodes based on $Li_{2.6}Co_{0.2}Cu_{0.2}N$ without and with HEMM at the first and the second cycle. The inset figure is Cycling performance of the electrodes of the $Li_{2.6}Co_{0.2}Cu_{0.2}N$ under different preparations.

2.3.3 Novel composite electrodes based lithium transition metal nitrides

1. Carbonaceous materials-lithium metal nitrides composites

MCMB is a kind of graphitic carbon and currently used as anode material in the commercial Li-ion batteries. The composite consisting of MCMB and $Li_{2.6}Co_{0.4}N$ was developed via HEMM. SEM observation on the composite reveal that after ballmilling the $Li_{2.6}Co_{0.4}N$ powders are severely smashed into nano- or submicro- scale, and dispersed and adhered compactly on the surface of the MCMB particles, as shown in Fig.18. Such morphology is favorable for the electrochemical kinetics of the $Li_{2.6}Co_{0.4}N$ particles by adopting MCMB as an appropriate electron-conductive matrix. MCMB has a low reactive potential at ca.0.1 V vs. lithium and a reversible capacity of 310 mAh g^{-1}. As compared, we can apparently observe the increased initial coulombic efficiency (100% vs.89%) and the increased reversible capacity

(450 mAh g^{-1} vs.310 mAh g^{-1}) for the $Li_{2.6}Co_{0.4}N$-MCMB composite electrode, as shown in the inset in Fig.19. The high faradic yield in the first cycle is dependent on the extraction capacity compensation of $Li_{2.6}Co_{0.4}N$. Compared with MCMB, the composite has a relatively enhanced safety due to the improved reactivity potential. The potential trends of the composite electrode reflect the mixing potential characteristics of these two types of active hosts. During cycling the $Li_{2.6}Co_{0.4}N$ yields charge potentials mainly in the realm of 0.6-1.1V vs.Li/Li^{+} and discharge potentials of 0.15-0.5 V vs.Li/Li^{+}. As a result, an obviously potential hystersis of the composite electrode between charge and discharge is still remarkable. Fig.19 shows the cycling performance of the electrodes based on the MCMB-lithium metal nitrides composite and the pure MCMB. The capacity-cycle curves deliver high stability, indicating a high reversibility of Li-insertion and extraction.

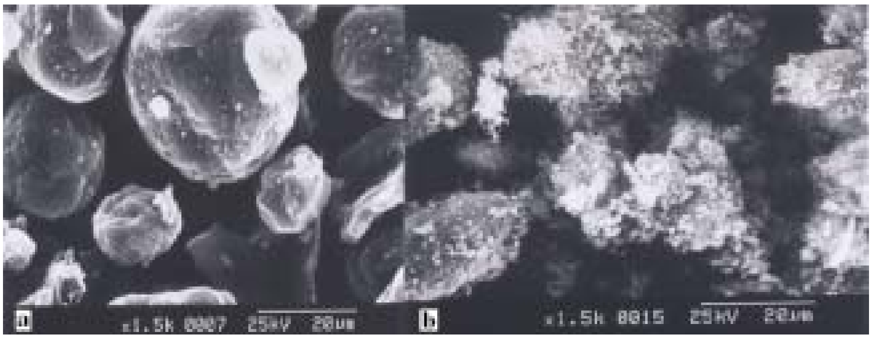

Fig.18. SEM photos of a) the mechanical mixture of MCMB-$Li_{2.6}Co_{0.4}N$ and b) the HEMM MCMB-$Li_{2.6}Co_{0.4}N$ composite prepared by HEMM.

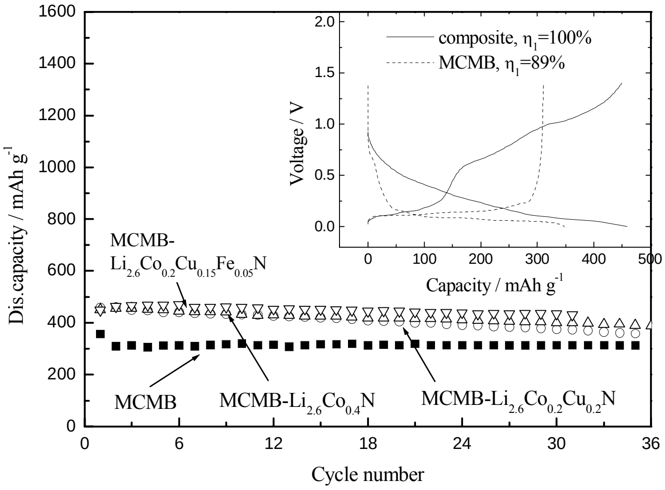

Fig.19. Cycling performance of the lithium metal nitrides-MCMB composites and the MCMB electrodes. The inset figure is charge and discharge curves of the $Li_{2.6}Co_{0.4}N$-MCMB composite and the MCMB electrodes at the first cycle.

2. Si-C-$Li_{2.6}Co_{0.4}N$ composites

Fig.20 shows charge and discharge profiles of the Si−graphite−$Li_{2.6}Co_{0.4}N$ composite synthesized from two HEMM processes. In the first discharge, the electrochemical behavior of the composite is only associated to silicon and graphite because fully lithiated $Li_{2.6}Co_{0.4}N$ has no extra vacancy for the initial Li intercalation. The capacity above 0.8 V from $Li_{2.6}Co_{0.4}N$ plays an important role for the compensation for the irreversible capacity. As a result, a high first-cycle efficiency of ca. 90 % was obtained. From the second cycle to the subsequent cycles, the voltage trends show high coincidence that indicates a good reversibility of Li insertion and extraction. Moreover, graphite in the composite is favorable for reducing the potential hysteresis arising from silicon and $Li_{2.6}Co_{0.4}N$ in charge and discharge. An XRD measurement was further conducted on the composite with respect to various charge-discharge stages, as shown in the inset (1) in Fig.20. Before cycling, the diffraction peaks reflected from silicon, graphite and $Li_{2.6}Co_{0.4}N$ can be distinguished (see a). The diffraction peaks from silicon and $Li_{2.6}Co_{0.4}N$ disappeared with the first discharge and charge,

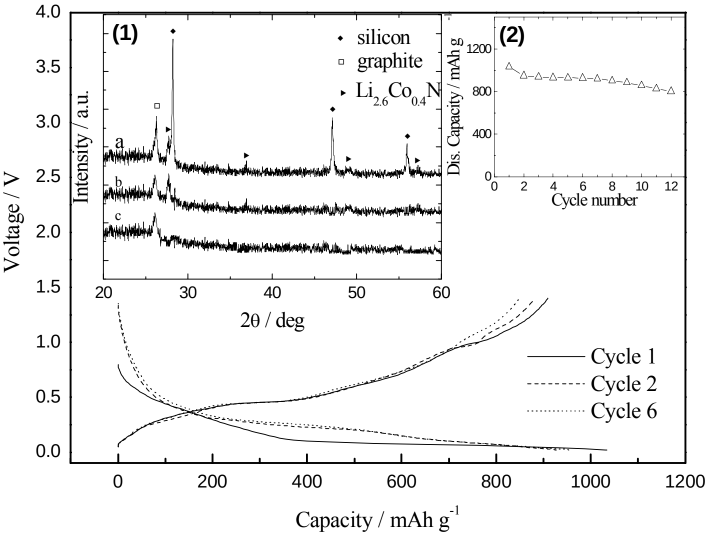

Fig.20. Charge and discharge curves of the Si−graphite−$Li_{2.6}Co_{0.4}N$ composite electrode at different cycles. The inset figure (1) is XRD patterns of the Si−graphite−$Li_{2.6}Co_{0.4}N$ composite electrode: (a) before charge and discharge, (b) after first discharge and (c) after first discharge. The inset figure (2) is cycling performance of the Si−C−$Li_{2.6}Co_{0.4}N$ composite.

as shown in b and c, respectively. The changed crystalline reflections remained same upon increasing of the cycle number. This result means that the electrochemical Li insertion and extraction make silicon and $Li_{2.6}Co_{0.4}N$ turn into amorphous. A SEM photo analysis reveals that all the components in the composite after HEMM tend to form large agglomerates, indicating that silicon could be highly dispersed and embedded within the ductile graphite−$Li_{2.6}Co_{0.4}N$ matrix. Obviously, such a granular structure is in favor for increasing the interfacial affinity of silicon with the matrix and leading to an ensured electrical contact. On the other hand, the low absolute volume effect of the composite using $Li_{2.6}Co_{0.4}N$ reduces the mechanical stress of the dispersed silicon. Thus, the composite demonstrates good cycling stability, as shown in the inset (2) in Fig.20. In comparison, silicon possesses the highest capacity of ca. 3.7 Ah g^{-1} in the first Li intercalation; but it suffers from a remarkable loss in the extraction capacity. By contrast, $Li_{2.6}Co_{0.4}N$ has a very low insertion capacity and very high extraction capacity. The Si−graphite−$Li_{2.6}Co_{0.4}N$ composite shows a large reversible capacity of ca. 1 Ah g^{-1} as three times as graphite and a high initial faradaic yield of 90 % that might lead to a high energy density of the lithium ion batteries.

3. $LiTi_2O_4$-lithium metal nitrides composites

The spinel $LiTi_2O_4$ demonstrates a high conductivity and an extremely constant charge/discharge potential versus lithium at ca.1.55V, as well as a reversible capacity of *ca.*170 mAh g^{-1}. The Li-intercalation potential of $LiTi_2O_4$ (*ca.*1.50V) is slightly higher than the Li-extraction potential of $Li_{2.6}Co_{0.4}N$ (*ca.*1.0V); therefore $LiTi_2O_4$ can extract lithium from $Li_{2.6}Co_{0.4}N$. Open potential of 0.95 V can be observed for the electrode when lithium in the $Li_{2.6}Co_{0.4}N$ was completely extracted. The suitable weight ratio of the nitrides to the $LiTi_2O_4$ in the electrode is dependent on the effective capacity and the molecular weight of the two active hosts. A possible chemical reaction between the two hosts is "$Li_{2.6-x}Co_{0.4}N + z\ LiTi_2O_4 \rightarrow Li_{2.6-x-z}Co_{0.4}N + z\ Li_2Ti_2O_4$ ($x + z \leq 1.6$)", where x means the lithium loss in the $Li_{2.6}Co_{0.4}N$ compared to the theoretical Li:Co ratio as 2.6:0.4, and z is the possibly extracted lithium related to $LiTi_2O_4$. Thus, in view of the fact that the introducing of HEMM enables the removal of part lithium in $Li_{2.6}Co_{0.4}N$ and $LiTi_2O_4$ has no capacity contribution in the electrode within a special potential range, the capacity utilization of the milled $Li_{2.6}Co_{0.4}N$ can be improved by reducing the contents of $LiTi_2O_4$. In the case of 22 wt% milled $Li_{2.6}Co_{0.4}N$ plus 70 wt% $LiTi_2O_4$, the first cycle efficiency is close to 100%. Fig.21 shows the charge and discharge curves of the electrode based on $Li_{2.6}Co_{0.2}Cu_{0.2}N$ and $LiTi_2O_4$ at different cycles. In general, a decreased particle size leads to an increased density. For example, the density of the mixture consisting of the separately milled $Li_{2.6}Co_{0.2}Cu_{0.2}N$ and $LiTi_2O_4$ is 3.2 g cm^{-3} according to the experimental data, versus 2.2 g cm^{-3} of the mixture based on the un-milled samples. Large volumetric capacity is dependent on the material's high specific capacity and density. In addition, $LiTi_2O_4$ can act as an inert-conducting additive in place of AB in the electrode within a potential range of 1.4V~0.01V vs.Li/Li^+. Thus, the composite electrode shows a comparative volumetric capacity. Taking $Li_{2.6}Co_{0.2}Cu_{0.2}N$ and $LiTi_2O_4$ as the active hosts, the volumetric capacity of the composite electrode is 798 mAh cm^{-3}, which is attractive compared to that of graphite (ca. 650-700 mAh cm^{-3}). The $Li_{2.6}Co_{0.2}Cu_{0.2}N$-$LiTi_2O_4$ composite electrode exhibits high cycling stability, as shown in the inset in Fig.21.

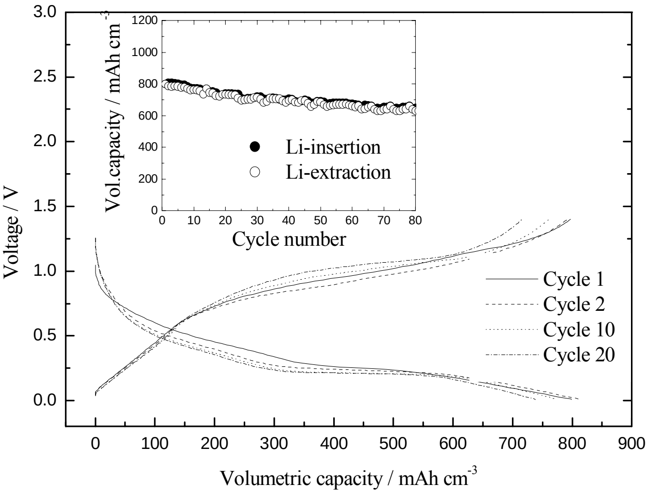

Fig.21. Charge and discharge profiles of the $Li_{2.6}Co_{0.4}N$-$LiTi_2O_4$ electrode at different cycles. The inset figure is the cycling performance.

4. Co_3O_4-lithium metal nitrides composites

Fig.22 shows charge and discharge curves of the Li/Co_3O_4 (a), Li/$Li_{2.6}Co_{0.2}Cu_{0.2}N$ (b) and Li/Co_3O_4-$Li_{2.6}Co_{0.2}Cu_{0.2}N$ (c) cells. The Co_3O_4 electrode had a large insertion capacity of 1100 mAh g^{-1} along with a potential plateau of 1.1 V in the first cycle. However, its capacity retention at the subsequent cycle was below to 180 mAh g^{-1} within the potential range of 0.01-1.4V. The electrochemical behavior of $Li_{2.6}Co_{0.2}Cu_{0.2}N$ was in contrast to that of Co_3O_4, which had a high extraction capacity of over 800 mAh g^{-1} with a potential plateau of 1.1 V but a very low first insertion capacity of around 200 mAhg^{-1}. In contrast, 100 % capacity retention at the first cycle was observed in the Co_3O_4-$Li_{2.6}Co_{0.2}Cu_{0.2}N$ composite electrode. XRD studies of the Co_3O_4-$Li_{2.6}Co_{0.2}Cu_{0.2}N$ composite on different charged states, as shown in Fig.23, revealed that the diffraction peaks from $Li_{2.6}Co_{0.2}Cu_{0.2}N$ and Co_3O_4 disappeared by soaking the composite in the electrolyte for 2h. The diffraction intensities remained constant with increasing charge depth and number of cycles. These results indicate that a thermodynamically spontaneous reaction between Co_3O_4 and $Li_{2.6}Co_{0.2}Cu_{0.2}N$ leads to an amorphous delithiated state of $Li_{2.6}Co_{0.2}Cu_{0.2}N$ and probably to form metallic Co and Li_2O. We propose that the reaction mechanism of the composite anode as follows:

$$Li_{2.6}Co_{0.2}Cu_{0.2}N + xCo_3O_4 \rightarrow Li_{2.6-8x}Co_{0.2}Cu_{0.2}N + 4xLi_2O + 3xCo \qquad (1)$$

$$Li_{2.6-8x}Co_{0.2}Cu_{0.2}N + zLi^+ + ze^- \rightarrow Li_{2.6-8x+z}Co_{0.2}Cu_{0.2}N \qquad (2).$$

Reaction (1) is a chemical reaction and reaction (2) is an electrochemical one. If $Li_{2.6-8x}Co_{0.2}Cu_{0.2}N$ is the composition of the fully charged state, then reaction (2) becomes reversible during charge and discharge even at the first cycle. We estimated x and z as 0.16 and 1.7, respectively. These values correspond to 60/40 weight ratio of $Li_{2.6-8x}Co_{0.2}Cu_{0.2}N/Co_3O_4$ and the reversible capacity of 477 mAh g^{-1}. We observed a first charge and discharge efficiency of 100% and a reversible capacity of ca. 500 mAh g^{-1} for the composite anode of 62.5 wt % $Li_{2.6-x}Co_{0.2}Cu_{0.2}N$ plus 37.5 wt % Co_3O_4 as shown in Fig. 1c. The high first cycle efficiency proposed with this anode can greatly extend the capacity utilization for the cathode. It is remarkable because the capacity of the conventional cathode materials in lithium batteries is less than 200 mA g^{-1}. The irreversible anode capacity in the first cycle requires an extra capacity of cathode active materials; thereby it inevitably depresses the total energy density of the batteries. Due to lithium metal nitride as the active hosts, such a composite demonstrate excellent capacity retention with cycling, as shown in the inset in 23.

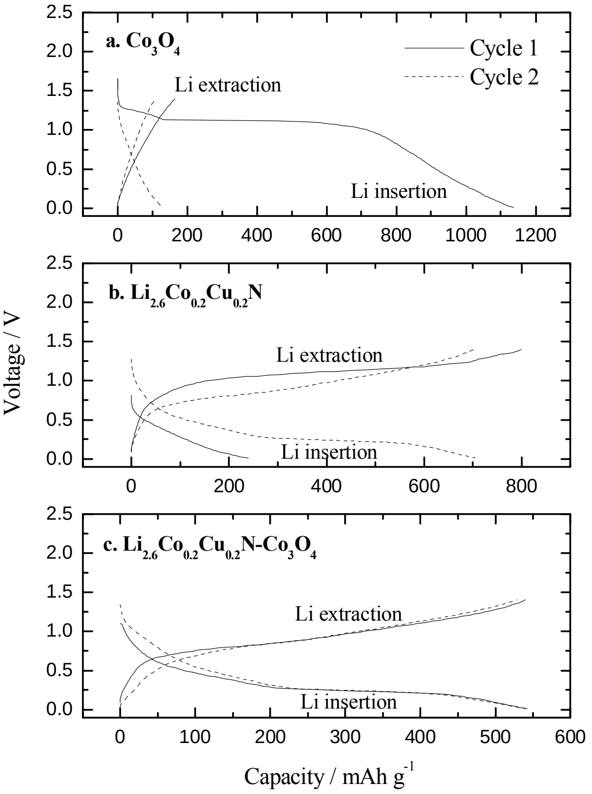

Fig.22. Charge-discharge curves of the cells: a) Co_3O_4 / electrolyte / Li, b) $Li_{2.6}Co_{0.2}Cu_{0.2}N$ / Electrolyte / Li and c) Co_3O_4 - $Li_{2.6}Co_{0.2}Cu_{0.2}N$ (37.5 - 62.5 wt. %) / electrolyte/ Li at room temperature.

2.4 Conclusions

In summary, we have developed a series of lithium mixed transition metal (co-doped) nitrides with high electrochemical capacity and good cyclability. For producing these compounds, a combination of a solid-state reaction under an appropriate temperature and a high-energy mechanical milling step was involved. Research reveals that the granular structure of the nitrides shows obvious effects upon the electrochemical behavior. The lithiated compounds can be used in several ways to form new composite electrodes which demonstrate high insertion capacity, 100 % first cycle efficiency and excellent capacity retention ability. Therefore, they are promising anode candidates for further Li-ion batteries.

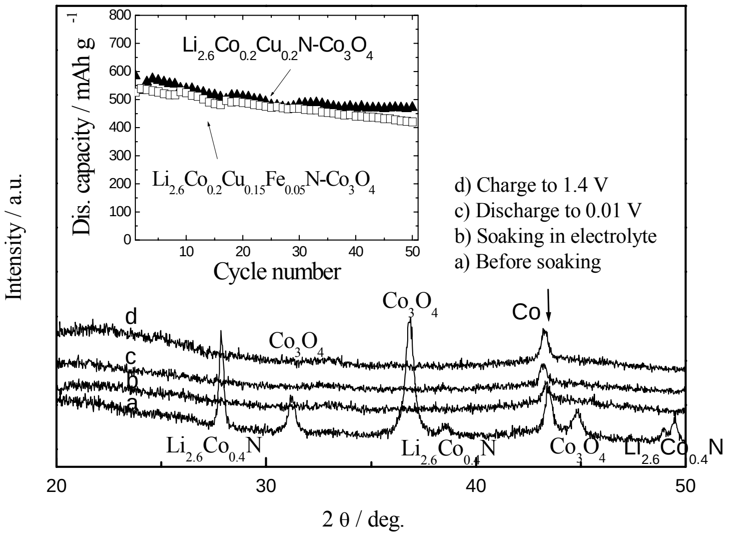

Fig.23. XRD patterns of the Co_3O_4-$Li_{2.6}Co_{0.2}Cu_{0.2}N$ composite electrode at different stages. The inset figure is cycling performance of the composites.

Part II Solid-state polymer electrolytes based system

1. Introduction

Since the discovery of ionic conductivity in the Poly (ethylene oxide) (PEO)-lithium salt composites, lithium-ion batteries based on such category of electrolytes has attracted worldwide attentions. In view of the high energy density and feasible design, all solid-state PEO rechargeable lithium batteries could be promising and ideal power source for EV&HEV [52]. So far, research has been extensively concentrated on two major points: the improvement of ionic conductivity of PEO-LiX complex at the relatively low temperature and the modification of interfacial characteristics between metallic lithium anode and polymer electrolytes. It is generally accepted that there is some instable issue between metallic lithium and PEO electrolytes caused by lithium dendrite grown [53,54]. Insertion hosts such as carbon, Li-alloy and Li-M-O, in place of lithium, present the promising alternative anodes that can avoid the above problem [55,56]. Unfortunately, carbon still cannot be adopted successfully in the PEO electrolytes due to the interfacial incompatibility, regardless of its wonderful electrochemical manners in the liquid system. On the other hand, some Li-M-O materials, e.g., spinel $Li_4Ti_5O_{12}$, demonstrate zero-strain effects for Li-insertion, resulting in long cycling life in the solid PEO electrolytes. Relatively low capacity and high Li-insertion potential of lithium titanates suffers loss of the comparable energy density. In contrast, for the large lithium storage capacity and low operating voltage close to lithium, Li-alloy could be considered as the appropriate candidate. It is believed that the morphology instability, which caused by the volume change of active hosts in association with lithium insertion, severely hinders the development of Li-alloy in both solid and liquid electrolytes. Decreasing particle size and adopting of multi-phase structure is favor for greatly enhancing the cyclability. Some positive results have been obtained, such as Li-Al electrode and interfacial layers of Li-Bi and Li-Pb alloys between lithium metal and solid polymer electrolytes [57,58]. However, the cycling performance of Li-alloy as anode in the solid PEO electrolytes is still poor.

Recently, we have developed a novel lithium ion cell consisting of the composite anode, such as SnSb-$Li_{2.6}Co_{0.4}N$, $SiO_{1.1}$-$Li_{2.6}Co_{0.4}N$, Co_3O_4-$Li_{2.6}Co_{0.2}Cu_{0.2}N$, and the $LiNi_{0.8}Co_{0.2}O_2$ cathode based on the solid PEO-$LiN(CF_3SO_2)_2$ electrolytes [59-63]. Such cells can offer large reversible anode capacity at 450 mAh g^{-1} and high working voltage, as well as an ensured safety without metallic lithium. In this part, the electrochemical performance of several types of novel anodes with the solid-state polymer PEO electrolytes are presented and discussed in detail.

2. Experimental

2.1 Active materials

$LiCo_{0.2}Ni_{0.8}O_2$ (typical particle size is 10 μm) was prepared by the normal solid state reaction. Ultrafine SnSb alloy powder (*ca.* 0.2 μm) was produced by chemical precipitation from aqueous solutions [12] and lithium metal nitrides was synthesized as mentioned above. Nickel powder (99.9%, ca. 0.03 μm), PEO (MW=6 × 10^5), $LiN(CF_3SO_2)_2$, $BaTiO_3$ (typical particle size, ca.0.1μm), PVDF (MW=534000) were commercially purchased. The Co_3O_4 powder (< 2 μm) was obtained by a decomposition reaction of $CoCO_3$ at 800 ^{0}C in air.

2.2 Polymer electrolyte and cathode film

All the procedure was carries out in the glove box protected by Ar. PEO electrolytes (Li/O ratio: 1/18) were prepared under the casting technique. A given weight of PEO (MW = 6 × 10^5) and $LiN(CF_3SO_2)_2$ was dissolved completely in anhydrous acetonitrile (AN). $BaTiO_3$ was dispersed homogeneously in the solution as filler. The viscous was strongly stirred overnight and cast into a Teflon dish. After AN was slowly and completely evaporated under N_2 flow, the obtained film was further dried at 90 ℃ under vacuum at least 8 h. Cathode films consisting of 52 wt% $LiNi_{0.8}Co_{0.2}O_2$, 10 wt% acetylene black(AB) and 38 wt% PEO-$LiN(CF_3SO_2)_2$ were prepared by the normal casting method similar to PEO film. The thickness of the cathode and PEO film was about 200 μm. The conductivities of the composite polymer electrolyte were observed as high as 1.7x10^{-3} S cm^{-1} at 80 ^{0}C and 0.82x10^{-3} S cm^{-1} at 65 ^{0}C.

2.3 Anode preparations

Different preparations were adopted and nominated as (a) dry mixing, (b) wet mixing, (c) hot pressing and (d) casting, respectively. For the dry mixing way, the electrode components were mechanically mixed in an agate mortar. In the case of method (b), the components were homogeneously mixed by the aid of Hexane as a disperser. Polymer binder was added and mixed after Hexane was entirely evicted. Mixtures prepared by (a) and (b) were pressed onto a 280-mesh stainless steel grid, which served as a current collector. Normally, area and thickness of the composite anodes were 0.55 cm^2 and 50-60 μm, correspondingly. Anode prepared by hot pressing was described as follows: PEO powders were carefully sieved and only the smallest particles were passed and used. Before hot pressing, the electrode components were homogeneously mixed and pressed directly onto Cu-foil (20 μm) in a steel mold at a temperature of 70-90℃ and pressure of 10-60 MPa. The press time was 0.5 h-6 h. The thickness of the obtained film was 60-90μm (including Cu-foil). The procedure of method (d) was similar to that of the PEO film preparation. PEO and $LiN(CF_3SO_2)_2$ (Li/O ratio: 1/18) were dissolved in AN solvent entirely. SnSb and conducting Ni powders were added and followed a strong stirring. At last, $Li_{2.6}Co_{0.4}N$ was added at 10 min before the casting. The viscous solution was cast onto a 280-mesh stainless steel grid and further dried at 90 °C under vacuum for 2 h.

2.4 Cell assembling and electrochemical measurement

To examine the cycling performance of the composite anode, half-cell was used and metallic lithium was utilized as counter electrode. The full cells were composed of the $LiNi_{0.8}Co_{0.2}O_2$ cathode and the SnSb-$Li_{2.6}Co_{0.4}N$ composite anode. Basically all the three layers, including composite anode, PEO electrolyte and cathode film (or lithium counter electrode), were stacked in coin type cells. A small constant pressure was kept inside cells by the means of the Ni foam as filler. Considering the corrosion instability of Al foil with $LiN(CF_3SO_2)_2$, stainless plate was used as cathode current collector. Thickness ratio of cathode film and current collector is about 1/3. Before assembly, the cathode film was tightly press on the current collector under slightly heat and pressure. Unless stated elsewhere, cycling properties tests were performed at a current density at 0.15 mA cm^{-2} and the working temperature was 65 °C. The voltage cutoff is 1.4-0.1V vsLi/Li^+ and 2.1-3.6V for half cell and full cell respectively. Before electrochemical test, the cells were preheated for 2 hrs at a temperature of 75°C. The discharge capacity was adopted for all figs, corresponding to Li-insertion into the SnSb-$Li_{2.6}Co_{0.4}N$ composite in half-cell and Li-extraction out from the SnSb-$Li_{2.6}Co_{0.4}N$ composite in full cell, respectively.

3. Results and discussion

3.1 Solid-state PEO cells based on SnSb-$Li_{2.6}Co_{0.4}N$ composite anode

Due to the drastic volume effects in association with Li intercalation into and extraction from SnSb hosts, the anode morphology stability, as well as the interfacial compatibility between the composite anode and the solid PEO electrolytes, dominate the cycling performance of the all solid-state cells. In general, the increased area of electrode is favorable for the electrochemical properties via decreasing the bulk resistance of the cell. However, the non-uniform dispersion of anode components prepared by dry mixing method tends to be aggravation accompanied with the enlarged electrode area. Non-uniform dispersion of lithium salt and nano-Ni conducting powder will cause the relatively low first cycle efficiency and the slightly increased voltage polarization. In addition, ultrafine SnSb particles with non-uniform distribution will form the large aggregation region and easily result in the local volume mismatch during charging and discharging. At last, rapid capacity decline is inevitable. Research reveals that the composite anode prepared by hot pressing and casting way demonstrates severe deterioration compared to dry mixing way.

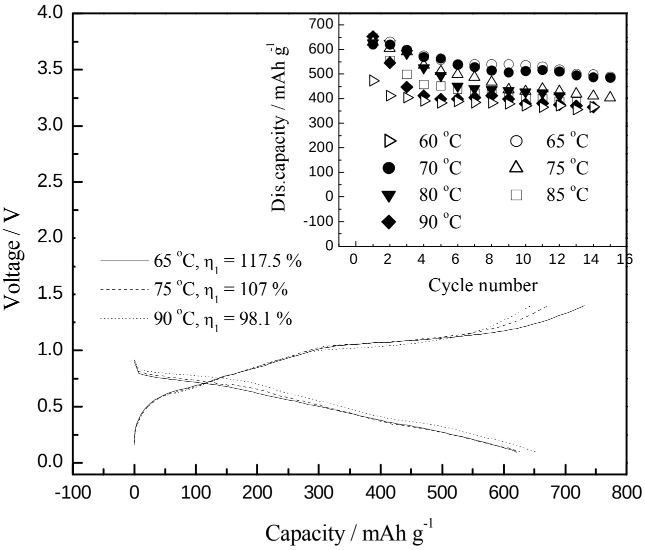

Fig.24. The first charge and discharge profiles of composite electrodes at different operating temperature. The inset figure is cycling performance of composite electrodes at different operating temperature.

Based on this, a solution stirring preparation by the aid of a dispersant, e.g., hexane, was introduced to achieve the homogeneous distribution of the electrode components. The cycling stability of the composite electrode prepared by the aid of solvent dispersion is obviously superior to those from other preparations. The observed results suggest that the appropriate anode preparation has an apparent effect upon the electrochemical behavior of the SnSb-$Li_{2.6}Co_{0.4}N$ composite anode. On the other hand, good electrode performance of the composite electrode requires a combination of suitable polymer binders. Poly(vinylidene fluoride) (PVDF) or poly(vinylidene fluoride) -hexafluoropropylene (PVDF-HFP) as binder in lithium ion batteries demonstrates enough binding ability, high mechanical and chemical stability even at elevated temperature. The electrochemical stable window of fluorinated polymers is as wide as 0 to 5 V vs. Li/Li^+. Moreover, these polymers are easer to be dispersed and can improve the adhesion between the active material and current collector. The mechanical strength of the composite electrode can be greatly reinforced by the use of PVDF as framework due to its strong binder ability for retraining the morphological instability in the Li-alloy processing, indicating that the function of fluorinated polymer and PEO-LiX as binder is mainly corresponding to sustain morphological stability and supply ionic channels within composite electrode respectively. Ionic conductivity predominates in the amorphous rather than crystalline regions of PEO electrolytes. The local relaxation and segmental motion of the polymer chains appears to be a requirement for lithium ion transport. The effect of operating temperature on mechanical strength and ionic movement of polymer electrolytes is contradictory. Therefore, it is reasonable that the SnSb-$Li_{2.6}Co_{0.4}N$ electrode performance exhibits a strong dependence on the environment temperature, as shown in Fig.24, in which the coulombic efficiency at the first cycle apparently decreases with increasing the temperature. It is noted that capacity lessen in the lithium extraction process is mainly attributed to shortness of voltage plateau near 1.1 V, which is related to $Li_{2.6}Co_{0.4}N$ active material. This indicates that the $Li_{2.6}Co_{0.4}N$ may lose some activity at high temperature in PEO-LiX system and it is the main reason for the reduced charge recovery in the subsequent cycles.

The deterioration of the mechanical performance of polymer PEO electrolyte at high temperature also takes part consequence. The temperature as a function upon the capacity-cycling behavior was shown in the inset in Fig.24. Below the melting point of PEO (ca. 65°C), the polymer electrolyte delivers enough mechanical strength and can hold good interfacial morphology stability between electrode and electrolyte. In addition, the relative rigidity of PEO-LiX at low temperature within composite electrode is favorable for restraining the volume expands of SnSb hosts for Li-insertion. However, low operating temperature corresponds to a poor interface contact and slow Li-transfer in both composite electrode and polymer electrolyte layers, resulting in a small capacity and unsteady cyclability. The capacity increases remarkably near PEO melting point due to adhesive interface contact and high ionic conductivity. It seems that such a cell system works poorly if the operating temperature continually grows over 75°C. At elevated temperature, sticky or even viscous property of the PEO-LiX in combination with the drastic volume effect of active SnSb particles will bring about a server mechanical instability of the electrode. The morphological change could be aggravated and hardly be recovered for the PEO-containing system above 75°C under strict pressure inside cells. The appropriate operating temperature for the SnSb-$Li_{2.6}Co_{0.4}N$ composite electrode is between 65 and 75°C. However such electrodes demonstrate a quite stable interfacial contact with polymer electrolytes during storage over a wide operating temperature. The interface resistance between composite electrode and solid electrolytes is acceptable even at 60 °C, as shown in the inset (1) in Fig.25, because the cell was preheated at a temperature 10°C higher than operating one before test. With increasing temperature, the impedance is greatly reduced, suggesting a significant improvement in the interfacial contact, as shown in the inset (2) in Fig.25. Dispersing $BaTiO_3$ in polymer binders may greatly reinforce the mechanical strength of PEO-LiX within composite electrode and, as a consequence, improves the morphology and cycling stability of whole electrode during charging and discharging. The typical charge and discharge profiles of the solid PEO Li-ion cell based on SnSb-$Li_{2.6}Co_{0.4}N$ composite anode and the $LiNi_{0.8}Co_{0.2}O_2$ cathode at 65°C are given in Fig.25. The $LiNi_{0.8}Co_{0.2}O_2$ cathode can deliver a reversible capacity about 140 mAh g^{-1} at appropriate working voltage scales in PEO-$LiN(CF_3SO_2)_2$-$BaTiO_3$ system, about one forth of that of the composite anodes. For full utilization of lithium storage capacity of composite anode, the weight of cathode has to be much over that of anode (4-5 times). A little increase of voltage plat from the first cycle to the following ones can be observed and it is mainly linked to the phase transfer of $Li_{2.6}Co_{0.4}N$ from crystal to amorphous state. It is attractive that a high coulombic efficiency over 94 % and a large reversible anode capacity about 500 mAh g^{-1} at the first cycle can be obtained in this system. Moreover, the capacity remains stable of above 400 mAh g^{-1} after 30 cycles under the limited lithium insertion. The capacity fade during cycling could be greatly prevented via the suitable charge-discharge control and the proper cell structure. A further improvement for cycling performance of the cells is still on the

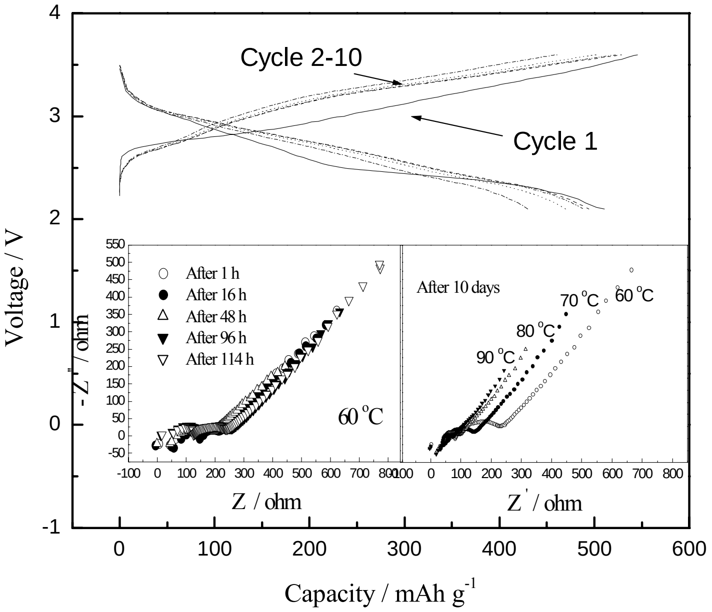

Fig.25. Charge and discharge profiles of coin type cell using $LiNi_{0.8}Co_{0.2}O_2$ cathode and composite anode in solid electrolytes at 65□. Voltage cut off: 2.1-3.6 V, $i_c=i_d=0.1$ mA cm^{-2}. The inset figure (1) is impedance performances of composite electrodes storage at 60□ at different time. The inset figure (2) is impedance performances of composite electrodes during storage at different operating temperature.

progression.

3.2 Electrochemical behavior of $SiO_{1.1}$-$Li_{2.6}Co_{0.4}N$ anode with the PEO electrolytes

The charge and discharge profiles of the $SiO_{1.1}$-$Li_{2.6}Co_{0.4}N$ composite electrode with the PEO electrolytes at different cycles are shown in the inset in Fig.26. The insertion capacity was increased to about 550 mAh g^{-1} at the second cycle, vs. 420 mAh g^{-1} at the first cycle. It is probably attributed to a reduced polarization caused by the improved electrochemical kinetics at the electrode interface compatibility. The voltage trends of the composite reflect mixing potential characteristics of $SiO_{1.1}$ and $Li_{2.6}Co_{0.4}N$ active materials. In fact, the capacity above 0.8 V from $Li_{2.6}Co_{0.4}N$ plays an important role for the compensation for the irreversible capacity. As a result, a high first cycle efficiency of ca.100% was obtained. The electrode compositions have an apparent influence upon the electrochemical behavior of the electrode, similar to that of the SnSb-$Li_{2.6}Co_{0.4}N$ electrode. Fig.26 shows the capacity change as a function upon the cycle number of the $SiO_{1.1}$-$Li_{2.6}Co_{0.4}N$ composite electrodes at various environment temperatures. The reversible capacity in the cycling beginning was improved with increasing the temperature due to the adhesive interface contact and high ionic conductivity. However, high temperature fast the capacity fading. It indicates that an aggravated decay in the mechanical strength of the PEO electrolytes can hardly endure the morphology instability arising from silicon. By contrast, PEO electrolyte at low temperature possesses a high mechanical stability with a low ionic conductivity that leads to a small capacity with good capacity retention. It was further found that dispersing sub-micro ceramic $BaTiO_3$ within the electrode is in favor for the cycling behavior of the composite electrode. Ceramic fillers, such as $BaTiO_3$ and Al_2O_3, can improve the mechanical performance of the flexible PEO electrolyte and stabilize the interfacial properties at elevated temperature. Furthermore, it can reduce the crystallizing tendency of the polymer electrolyte; thereby it enhances the ionic conductivity. With temperature increasing, the solid PEO-$LiN(CF_3SO_2)_2$ composite electrolyte turns into be serious sticky and fluid. The function of $BaTiO_3$ is to enhance the mechanical strength of the electrolyte components within the composite electrode that could maintain the electrode integrity. Research reveals that the suitable current density for this composite electrode in the solid PEO electrolytes is between 0.1 and 0.5 mA cm^{-2} after tradeoff capacity and capacity retention.

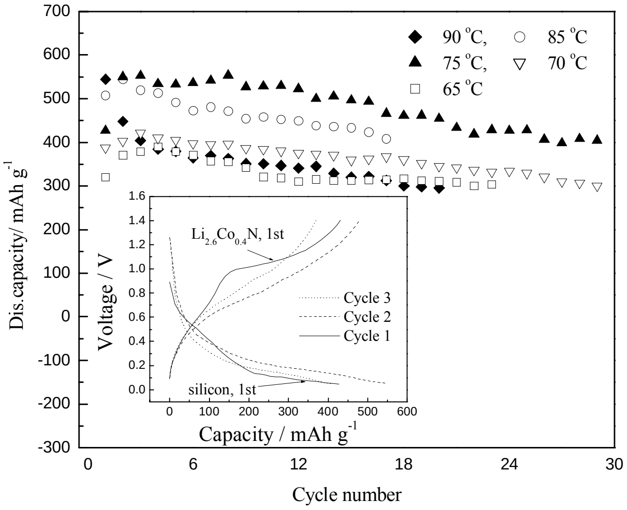

Fig.26. Cycling performance of the composite electrodes at different temperature. The inset figure is charge and discharge curves of the $SiO_{1.1}$-$Li_{2.6}Co_{0.4}N$ composite electrode at different cycles.

3.3 Electrochemical behavior and thermal performance of the Co_3O_4-$Li_{2.6}Co_{0.2}Cu_{0.2}N$

The Co_3O_4-$Li_{2.6}Co_{0.2}Cu_{0.2}N$ composite demonstrate reasonable interfacial compatibility with PEO electrolytes and thus good electrochemical behavior. The capacity changes, as a function of cycling, for different anodes with the solid PEO-based polymer electrolytes are shown in Fig. 27. The reversible capacity of graphite was below 200 mAh g^{-1} and the charge and discharge efficiency in the first several cycles was extremely low. Moreover, its capacity retention suffered from an obvious fading during cycling. The SnSb-$Li_{2.6}Co_{0.4}N$ anode had a large capacity of over 600 mAh g^{-1} and high coulombic efficiency of ca. 100 % in the first cycle. However, a gradual deterioration in the cycling performance was always observed due to the volume effects of alloys. The capacity fade was significantly suppressed for the $Li_{2.6-x}Co_{0.2}Cu_{0.2}N$-$Co_3O_4$ anode and estimated to be only about 0.37%/cycle during cycling. The charge and discharge profiles of the $Li_{2.6-x}Co_{0.2}Cu_{0.2}N$-$Co_3O_4$ anode at 65 ℃ as shown in the inset in Fig.27 indicate that the charge-discharge efficiency was almost 100% and lithium can be intercalated and extracted with a high reversibility. In general, the safety of small size lithium-ion cells under normal use is well established. In contrast, the safety of the large size lithium-ion batteries is still questionable, especially in cases of abusive use. Safety of lithium ion batteries is mainly related to the thermal reactivity of the electrode components. We found that specific reaction heats, which indicates the thermal stability and safety of the battery system, for the $Li_{2.6}Co_{0.2}Cu_{0.2}N$-$Co_3O_4$ anode charged up to 0.01 V vs. Li/Li^+ was estimated to be 1.1 J mAh^{-1}. Those for $Li_{2.6}Co_{0.2}N$-SnSb anode was 2.75 J mAh^{-1}. The specific reaction heat for lithium metal and PEO electrolyte (1:1 weight ratio) is 1.24 J mAh^{-1}. However, in practice, for the case of a lithium metal anode, an excess amount of lithium metal, at least four times compared to the cathode capacity, should be used because of the dendrite formation on the anode. Therefore, the reaction heat of lithium metal with PEO electrolytes was estimated to reach 4.96 J mAh^{-1} or higher. Therefore, the Li$_{2.6}$Co$_{0.2}$Cu$_{0.2}$N-Co$_3$O$_4$ anode shows the lowest reaction heat, indicating that the novel anode has potential applications in the large size rechargeable lithium-ion batteries for EV & HEV.

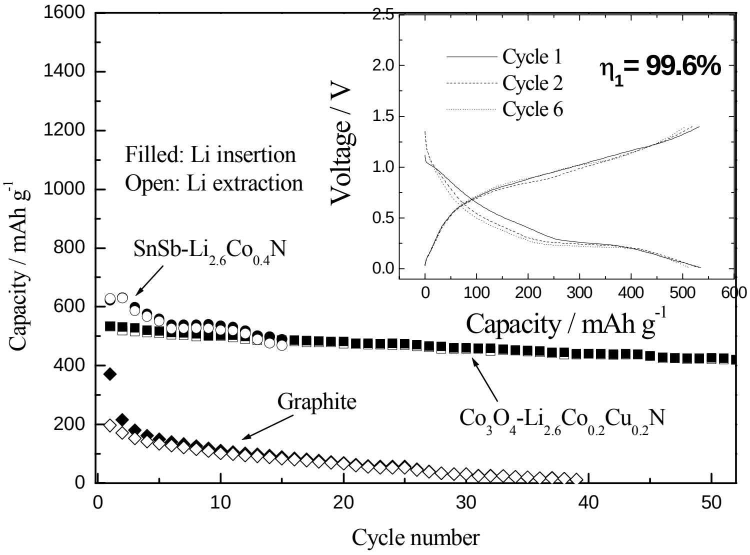

Fig.27. Cycling performance of SnSb-Li$_{2.6}$Co$_{0.4}$N, Co$_3$O$_4$-Li$_{2.6}$Co$_{0.2}$Cu$_{0.2}$N and graphite with PEO electrolytes vs. Li at 65°C. The inset figure is charge and discharge profiles of the Co$_3$O$_4$-Li$_{2.6}$Co$_{0.2}$Cu$_{0.2}$N electrode.

3.4 Conclusions

Anode material, which possesses large capacity density, high first cycle efficiency and low reaction heating with the PEO electrolytes, is the key for developing lithium polymer rechargeable batteries that proposed for extremely demanding applications such as electric vehicles (EV) and hybrid electric vehicles (HEV). By this motivation, we have developed series novel composite anode which show good electrochemical behavior with the PEO electrolytes. We are at present investigating the performance of the all solid-state PEO cells with these proposed novel anodes and some typical high potential cathodes

Acknowledgements

Part of the research work was carried out under a collaboration program of Mie University and Genesis Research Institute (Nagoya), and part was sponsored by new Energy and Industrial Technology Development Organization, Japan.

References

[1] J.-M. Tarascon and M. Armand, Nature 414,359-367 (2001)
[2] S. Eckfeld, J.E. Manders, M.W. Stevenson, J. Power Sources 5105 (2003) 1-8
[3] S. Levaesseur,M.Menetrier,C. Delmas, J. Electrochem. Soc. 149 (2002) A1533.
[4] A.K. Padhi, K.S. Nanjundaswamy, J.B. Goodenough, J. Electrochem.Soc. 144 (1997) 1188
[5] K. Sato, M. Noguchi, A. Demachi, N. Oki, M. Endo, Science 264 (1994) 556
[6] M. Winter, J.O. Besenhard, Electrochimica Acta 45, (2003) 31
[7] M. Nishijima, T. Kagohashi, N. Imanishi, Y. Takeda, O. Yamamoto and S. Kondo, Solid State Ionics, 83 (1996) 107
[8] P. Poizot, S. Laruelle, S. Grugeon, L. Dupont, J-M. Tarascon, Nature 407 (2000) 496
[9] Y. Idota, T. Kubota, A. Matsufuji, Y. Maekawa, T. Miyasaka, Science 276 (1997) 1395
[10] A. N. Dey, J. Electrochem. Soc., 118, 1547 (1971).
[11] J. O. Besenhard, M. Hess and P. Komenda, Solid State Ionics, 40/41 (1990) 525
[12] J. Yang, M. Winter and J. O. Besenhard, Solid State Ionics, 90 (1996) 281
[13] W.B. Xing, A.M. Wilson, K. Eguchi, G. Zank, J.R. Dahn, J. Electrochem. Soc. 144, 2410 (1997)
[14] A.M. Wilson, G. Zank, K. Eguchi, W. Xing, J.R. Dahn, J. Power Sources 68, 195 (1997)
[15] H. Kim, J. Choi, H.J. Sohn, T. Kang, J. Electrochemical Society 146, 4401 (1999)
[16] H. Li, X.J. Huang, L.Q. Chen, G.W. Zhou, Z. Zhang, D.P. Yu, Y.J. Mo, N. Pei, Solid State Ionics 135, 181 (2000)
[17] A. Netz, R.A. Huggins, W. Weppner, J. Power Sources 5271, 1 (2003)
[18] O. Mao, R.L. Turner, I.A. Courtney, B.D. Fredericksen, M.I. Buckett, L.J. Krause, J.R. Dahn, Electrochem. Solid-State Lett., 2 (1999) 3
[19] II-S. Kim, P.N. Kumta, G.E. Blomgren, Electrochem. Solid-State Lett., 3 (2000) 493
[20] II-S. Kim, G.E. Blomgren, P.N. Kumta, Electrochem. Solid-State Lett., 6 (2003) A157
[21] II-S. Kim, G.E. Blomgren, P.N. Kumta, J. Power Sources, 130 (2004) 275

[22] H.Y. Lee, S.M. Lee, J. Power Sources, 112 (2002) 649
[23] N. Dimov, K. Fukuda, T. Umeno, S. Kugino, M. Yoshio, J. Power Sources 5030, 1 (2002)
[24] X.Q. Yang, J. McBreen, W.S. Yoon, M. Yoshio, H.Y. Wang, K.J. Fukuda, T. Umeno, Electrochemistry Communications 4, 893 (2002)
[25] N. Dimov, S. Kugino, M. Yoshio, Electrochimica Acta 48, 1579 (2003)
[26] A.M. Wilson, J.R. Dahn, J. Electrochem. Soc. 142, 326 (1995)
[27] D. Larcher, C. Mudalige, A.E. George, V. Porter, M. Gharghouri, J.R. Dahn, Solid State Ionics 122, 71 (1999)
[28] Y. Liu, K. Hanai, J. Yang, N. Imanishi, A. Hirano, Y. Takeda, Solid State Ionics, 168 (2004) 61.
[29] Y. Liu, K. Hanai, J. Yang, N. Imanishi, A. Hirano, Y. Takeda, Electrochem. Solid-State Lett., 7 (2004) A369.
[30] Y. Liu, K. Hanai, T. Matsumura, N. Imanishi, A. Hirano and Y. Takeda, Electrochem. Solid-State Lett., 7 (2004) 12
[31] K. Hanai, Y. Liu, N. Imanishi, T. Ichikawa, A. Hirano and Y. Takeda, J. Power Sources, in press
[32] Y. Liu, K. Hanai, N. Imanishi, A. Hirano, T. Matsumura and Y. Takeda, Solid State Ionics, in press.
[33] G.X. Wang , L. Sun, D.H. Bradhurst, S. Zhong, S.X. Dou, H.K. Liu, Journal of Alloys and Compounds 306 (2000) 249
[34] J. Yang, Y.Takeda, N.Imanishi, C.Capiglia, J.Y.Xie, O.Yamamoto, Solid State Ionics 152-153 (2002) 125
[35] M.N. Richard, J.R. Dahn, J. Electrochem. Soc. 146 (1999) 2068
[36] J. Yamaki, H. Takatsuji, T. Kawamura, M. Egashira, Solid State Ionics 148 (2002)241
[37] M. Nishijima, T. Kagohashi, N. Imanishi, Y. Takeda, O. Yamamoto, J. Power Sources, 68 (1996) 510
[38] S. Suzuki, T. Shodi and J. Yamaki, J. Phys. Chem. Solids, 59 (1998) 331
[39] T. Shodi, S. Okada, S. Tobishima and J. Yamaki, J. Power Sources 68 (1997) 515
[40] T. Shodi, Y. Sakurai and T. Suzuki, Solid State Ionics 122 (1999) 85
[41] T. Y. Kim, M. G. Kim, J. M. Lee, T. Kang and H. J. Sohn, Electrochemical and Solid-State Letters, 5 (2002) A103
[42] Y. Takeda, M. Nishijima, M. Yamahata, K. Takeda, N. Imanishi and O. Yamamoto, Solid State Ionics, 130 (2000) 61
[43] J. Yang, Y. Takeda, N. Imanishi and O. Yamamoto, J. Electrochem. Soc., 147 (2000) 1671
[44] J. Yang, Y. Takeda, N. Imanishi and O. Yamamoto, Electrochimica Acta, 46 (2001) 2659
[45] Y. M. Kang, S. C. Park, Y. S. Kang, P. S. Lee and J. Y. Lee, Solid State Ionics 156 (2003) 263
[46] Y. Liu, K. Horikawa, M.Fujiyosi, N. Imanishi, A. Hirano and Y. Takeda, J. Electrochem. Soc., 151 (2004) A1450
[47] Y. Liu, T. Matsumura, N. Imanishi, T. Ichikawa, A. Hirano, Y. Takeda, Electrochemistry Communications 6 (2004) 632
[48] Y. Liu, K. Horikawa, M. Fujiyosi, N. Imanishi, A. Hirano and Y. Takeda, Electrochimica Acta 49 (2004) 3487
[49] Y. Liu, K. Horikawa, M. Fujiyoshi, T. Matsumura, N. Imanishi and Y. Takeda, Solid State Ionics, 172 (2004) 69
[50] Y. Liu, N. Imanishi, A. Hirano, T. Matsumara and Y. Takeda, Electrochem. Solid-State Lett., in submission
[51] Y. Liu, K. Hanai, K. Horikawa, N. Imanishi, A. Hirano and Y. Takeda, Materials Chemistry & Physics, in press
[52] Y.Aihara, M.Kodama, K.Nakahara, H.Okise, K. Murata, J.Power Sources. Vol.65 pp.143-148 (1997).
[53] F. Croce, B. Scrosati, J. Power Sources.Vol.43-45, pp.9-12 (1993).
[54] I.M. Ismail, U. Kadiroglu, N. D. Gray, J. R. Owen, in: Electrochemical Society Meeting Abtracts, San Antonio, TX, Oct. 6-12 Vol. 96-2,1999, Abstract 63.
[55] D. Fauteux and R. Koksbang, J. Appl. Electrochem. Vol.23, pp.1-6 (1993).
[56] J. O. Besenhard, J. Yang and M. Winter, J. Power Sources 68 (1997) 87
[57] A. Belanger, M. Robitaille, US patent 4652506, 1989.
[58] M. Hiratani, K. Miyauchi, T. Kudo, in: Int.Conf Solid State Inoics, Garmish 28-30 (1988) 1431
[59] J. Yang, Y. Takeda, Q. Li, N. Imanishi, O. Yamamoto, J. Power Sources 90 (2000) 64
[60] J. Yang, Y. Takeda, Q. Li, N. Imanishi, O. Yamamoto, J. Power Sources 97-98 (2001) 779
[61] J. Yang, M. Wachtler, M. Winter, J. O. Besenhard, Electrochem. Solid State Lett. 2 (1999) 161.
[62] Y. Liu, J. Yang, N. Imanishi, A. Hirano, Y. Takeda, and O. Yamamoto, J. Ceramic Society of Japan 112 (2004) s638.
[63] Y. Liu, J. Yang, N. Imanishi, A. Hirano, Y. Takeda and O. Yamamoto, J. Power Sources, in press